Wet compressor performance analysis using a cycle energy balance model

Master Thesis

by

Jesper Overbeeke

to obtain the degree of Master of Science
at the Delft University of Technology
to be defended publicly on August 27, 2024 at 11:00

Thesis committee:

Prof. dr. K. Hooman
E. Zanetti, PhD
Dr. M. Ramdin

Project Duration: September, 2023 - August, 2024
Student number: 4555503

Faculty of Mechanical, Maritime and Materials Engineering (3mE) · Delft University of Technology

Abstract

With the adoption of the Paris Agreement, 196 countries worldwide committed to the limitation of the global temperature rise. In order to achieve this goal more energy needs to be produced in a sustainable way. However, the industrial sector is still mainly fossil driven and therefore has to adapt to be able to utilize sustainable produced power, which most often is in the form of electricity. More than a quarter of the total heating demand is in the $100\,^{\circ}$C to $200\,^{\circ}$C range. In this temperature range heat pumps are a strong alternative to fossil fuels. Heat pumps can absorb energy from a low temperature heat source and deliver it at a higher, usable temperature.

Various technologies for waste heat recovery were investigated in this thesis. It was identified that existing heat pump technologies are suitable to upgrade waste heat, but are limited to lower temperatures of around $120\,^{\circ}$C. This limitation is mostly due to the high compressor discharge temperatures, which degrade the lubrication oil. Compression resorption heat pumps utilizing wet compression (CRHP's) limit the superheating during compression and are able to operate oil free, because the working fluid acts as a lubricant. This increases the achievable compressor discharge temperature. The wet compression however is not yet a mature technique and an isentropic efficiency of 70% is required to be competitive with existing technologies. Absorption cycles show promising results for upgrading waste heat due to their non-isothermal heat source and sink, which can be matched to the waste heat temperature.

At the Process and Energy lab experiments have been performed on a wet compressor using an ammonia water mixture. This thesis proposes a new method of analysing existing experimental data through a cycle energy balance model. In order to create a model of the experimental setup, four limitations of the setup were identified. First the influence of the gap seal flow, which is the flow from the high pressure to the lower pressure side of the compressor. Second, the mixture inside the compressor can not be assumed homogeneous, which means that both phases are not in equilibrium. Third, there is cooling oil flowing through the compressor housing which cools the process side, this results in a non-adiabatic compression. Finally the pressure drop on the high pressure side is not measured, resulting in an error when calculating the composition of the working fluid.

In order to model these limitations a model of the experimental setup was created in Aspen Plus. This model was supplemented with Matlab code to account for the non-equilibrium compression as well as the pressure drop and gap seal flow. Empirical relations were used to determine the heat and mass transfer between the phases during compression. The isentropic efficiency of the modelled compressor was varied until the output matches the input indicating that the steady state solution has been found. The influence of the non-adiabatic compression and the gap seal flow seem to have a significant impact on compressor performance. It was found that the compressor has the highest volumetric and isentropic efficiency when the inlet vapor quality is around 0.85 and the performance decreases with higher vapor qualities. Isentropic efficiencies of up to 0.88 were calculated. The results were compared against previous analysis of the same experimental data which used different assumptions and did not consider the whole cycle.

Finally, a case study was performed to analyse the applicability of heat pump technology to upgrade waste heat in a paper recycling plant. A conventional vapor compression heat pump (VCHP) and an electric boiler were compared to a CRHP. To deal with the uncertainty of wet compression performance a range of isentropic efficiencies were considered as well as different ammonia concentrations. The CRHP proved to be energetically and economically viable and outperformed both the VCHP and electric boiler in this case study.

Contents

Nomenclature

Abbreviations

COP	Coefficient of Performance
CRHP	Compression Resorption Heat Pump
GWP	Global Warming Potential
HACHP	Hybrid Absorption Compression Heat Pump
HTHP	High Temperature Heat Pump
IHX	Internal Heat Exchanger
ODP	Ozone Depletion Potential
RPM	Rotations Per Minute
TCHP	Transcritical Vapor Compression Heat Pump
VCHP	Vapor Compression Heat Pump

Greek symbols

Φ	Two phase multiplier	-
α	Void fraction	-
η	Efficiency	-
μ	Viscosity	Pa · s
ϕ	Male rotor angle	°
ζ	Darby friction factor	-

Roman symbols

$\dot{m}$	Mass flow	kg/s
$\dot{Q}$	Rate of heat transfer	W
$\dot{W}$	Rate of work	W
A	Area	m^2
C	Installed equipment cost	€
c_p	isobaric heat capacity	J/(kg · K)
D	Diameter	m
f_m	Fanning friction factor	-
Gr	Grashof number	-
H	Total enthalpy	J
h	Specific enthalpy	J/kg
k	Heat conductivity	W/(m · K)
L	Length	m
m	Mass	kg
N	Rotational speed	RPM
Nu	Nusselt number	-
p	Pressure	bar
Pr	Prandtl number	-
q	Vapor quality	-
R	Thermal resistance	
r	Radius	
Re	Reynolds number	-
s	Specific entropy	J/(kg · K)
T	Temperature	K
t	Thickness	m
U	Thermal conductance	
u	Velocity	m/s
V	Volume	m^3
X	Ammonia mass fraction	-
x	Distance	m

Subscripts

a	Acceleration
abs	absorber
ad	Adiabatic
bend	Pipe bend
cav	Cavity

ch	Compressor housing
cold	Cold
comp	Compressor
cr	Cross section
cw	Cooling water
dis	Discharge
dr	Driving
elec	Electric
evap	Evaporation
fr	Friction
g	Gravitational
hot	Hot
hx	Heat exchanger
in	In
is	Isentropic
k	Control volume k
L	Liquid
m	Mean property
n	Iteration number
O	Oil
out	Out
pump	Pump
S	Solid
sep	Separator
sink	Heat sink
source	Heat source
str	Straight section
sub	Subcooler
suc	Suction
sys	System
T	Average property of vapor and liquid
tr	Electrical tracing
turb	Turbine
V	Vapor
wh	Waste heat

List of Figures

1 Introduction

1.1. Background

On 12 December 2015, 196 countries adopted the legally binding international treaty on climate change under the UNFCCC, better known as the Paris Agreement [1]. The aim of the Paris Agreement is to limit the global temperature rise to 1.5°C and at least keep it below 2°C. In order to limit global warming to 1.5°C the greenhouse emissions have to decrease by 43 % by 2030. In order to achieve this goal sustainable energy production has to be increased as well as a the reduction of energy being used by making existing processes more efficient.

As can be seen in figure 1.1 the mayor part of primary energy usage today is still not sustainable

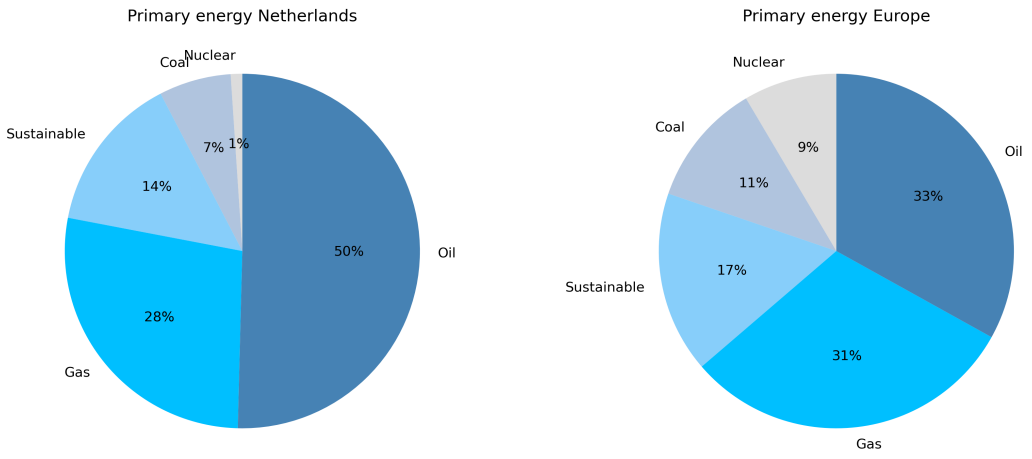

Figure 1.1: Left: primary energy usage in the Netherlands, right: primary energy usage Europe [2]

It is therefore important that not only the primary energy source changes, but also that the consumers adapt to the change in final energy form. According to Eurostat [3] the industry is responsible for 25.6% of the European total final energy consumption. In 2021 this was equivalent to 2800 TWh.

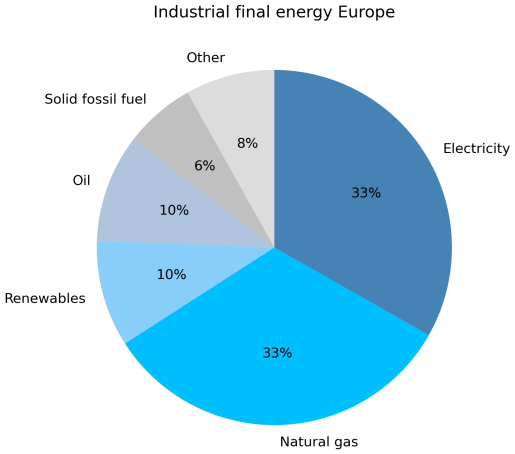

Figure 1.2: Industrial final energy usage Europe [3]

As can be seen in figure 1.2 the final energy consumed by industry was only 33.2% electric with 48.9% being fossil. This means that a lot still has to be done to make this sector more sustainable. According to Boer et al. 66% of the industrial energy use is used for process heating, which is mainly fossil driven [4]. Of this process heating 27% is in the range of $100°$C $-200°$C. Worldwide this is equal to approximatly 6000 TWh [5].

In table 1.1 the temperature ranges of a few relevant industries are shown.

Sector	**Process**	**Temperature range [°C]**
Paper	Drying	90-240
	Boiling	110-180
Food & Beverages	Drying	40-250
	Evaporation	40-170
Chemicals	Destillation	100-300
	Compression	110-170
Plastic	Injection molding	90-300

Table 1.1: Process temperatures in industry [5]

It can be seen that there are several applications where high temperature heat pumps have potential. In 2019 Schlosser et al. reviewed the potential of large-scale heat pumps for industrial applications [6]. It was concluded that the industrial heat pumps have a large potential once the fossil fuel gets more expensive and electricity production gets more sustainable. In 2020 Gudjonsdottir and Infante Ferreira investigated the potential of wet compression resorption heat pumps [7]. It was concluded that compression resorption heat pumps are a promising option to upgrade waste heat streams, even for large temperature glides. It is however highly dependent on the price of gas and electricity.

1.2. Heat pump fundamentals

The fundamentals of a heat pump are best explained for the case of a vapor compression heat pump (VCHP). These days everyone had a vapor compression heat pump in their home, the refrigerator. In figure 1.3 a overview of a VCHP is shown.

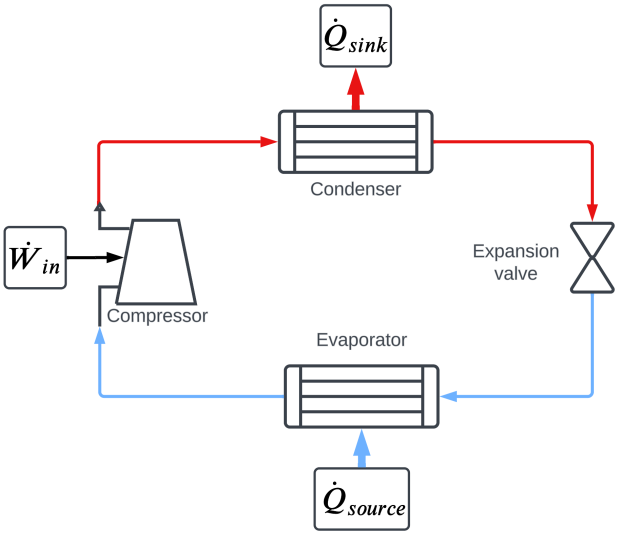

Figure 1.3: Layout VCHP

The VCHP uses the concept that the boiling point of a pure substance increases with pressure. The heat pump has a low and high pressure side. At the high pressure side the compressed vapor condenses at a high temperature, during this condensation the condenser heats up the cooling water. This is shown as $\dot{Q}_{sink}$. At the end of the condensation all the vapor has been converted to liquid. This liquid gets throttled by the expansion valve. This expansion lowers both the temperature and pressure as well as decreasing the vapor quality to almost zero. Due to the lower pressure the liquid can be evaporated in the evaporator at a much lower temperature. This is in turn able to cool down a stream. This is shown as $\dot{Q}_{source}$. This cycle is driven by the compressor which has power $\dot{W}_{in}$. Energy is conserved as can be seen in equation 1.1.

$$\dot{Q}_{source} + \dot{W}_{in} = \dot{Q}_{sink} \tag{1.1}$$

1.2.1. Heat pump performance

Cycle performance is quantified by the coefficient of performance (COP). The COP relates the usable heat output from the cycle to the work necessary to drive the cycle. In the case of a heat pump that is used for heating the COP can be calculated as shown in in equation 1.2.

$$COP = \frac{\dot{Q}_{sink}}{\dot{W}_{in}} \tag{1.2}$$

As can be seen in equation 1.1 the $\dot{Q}_{sink}$ is always larger than $\dot{W}_{in}$ therefore the COP is larger than 1. Comparing this to for example an electronic heater with a maximum efficiency of 100% shows the huge potential of heat pumps.

2

Theory

In this chapter several technologies for waste heat recovery will be investigated. First the vapor compression heat pump will be explained. After that the compression resorption heat pump with and without wet compression will be thoroughly analyzed. Special attention will be given to the wet compressor. At the end the organic rankine cycle, a heat engine and the transcritical vapor compression heat pump will be shortly reviewed.

2.1. Vapor compression heat pump

The vapor compression heat pump (VCHP) has been introduced in section 1.2. The layout of a VCHP is shown in figure 1.3. VCHP's have been used for a long time and is a well developed technology. VCHP's can be used with temperatures up to $150\,^{\circ}$C but most commercial options are limited to $120\,^{\circ}$C [8]. The limiting factors for VCHP's are the large pressures and discharge temperatures that occur if used for high temperature applications. The large pressures drive up the equipment cost, resulting in longer payback times. The high discharge temperatures result in degradation of the lubrication oil that has to be used in order to lubricate the compressor. This causes problems for the lubrication of the compressor. Lubrication oil can also accumulate on the heat exchanger resulting in decreased performance [9].

A few alterations to the VCHP can be used to enhance the operating window and increase performance. Such as internal heat exchange between suction gas and subcooled liquid, vapor injection into the compressor and two stage configurations. Two stage operation allows for less superheating and therefore higher temperature lifts. In figure 2.1 a cascade VCHP with internal heat exchange is shown [8].

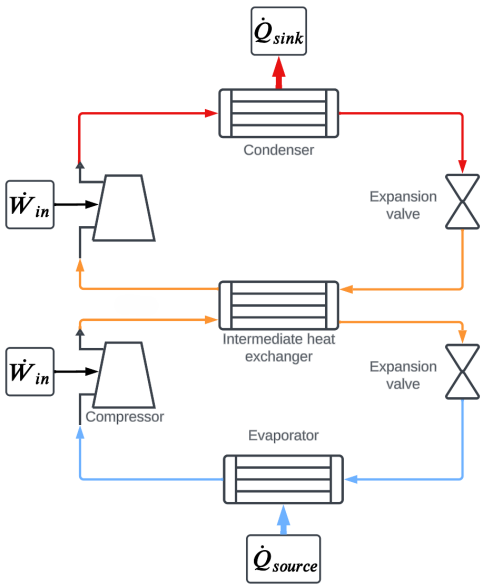

Figure 2.1: Cascade VCHP

In figure 2.2 the T-s diagram of an ideal VCHP is shown. It can be seen that the compression between 1 and 2 is isentropic. The difference between 2 and 2a is the amount of superheating. The condensation between 2a and 3 and the evaporation between 4 and 1 is isothermal.

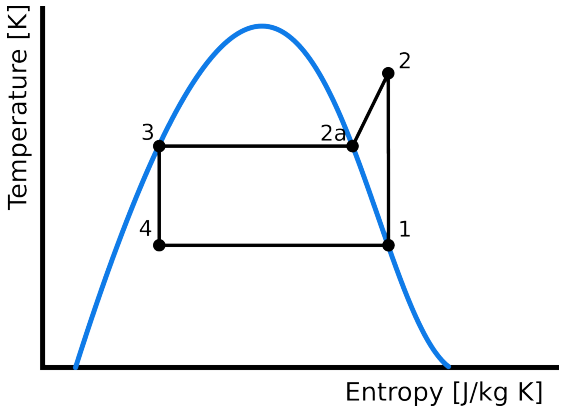

Figure 2.2: T-s diagram VCHP

To summarize a overview of the advantages and limitations of VCHP will be given:

Advantages
The main advantages of VCHP are:

- Mature technology [10]
- With cycle optimizations able to reach temperatures up to $150\,^{\circ}$C [8]

Limitations
The main limitations of VCHP are:

- Primarily uses working fluids with high GWP [11]
- High compressor discharge temperatures ($180\,^{\circ}$C) become problematic because lubrication oil breaks down [12]
- High pressure ratio needed to achieve high temperature lift [13]
- Cycle optimizations increase cost and complexity

2.2. Compression resorption heat pump with dry compression

The compression resorption heat pumps with dry compression will be named hybrid absorption compression heat pumps(HACHP) in this paper. First the cycle will be explained, after that existing research will be analysed and the advantages and limitations will identified.

Cycle
The simplest HACHP cycle is based on the Osnabrück cycle [14]. The hybrid absorption compression heat pump (HACHP) is different to the traditional VCHP because it uses a zeotropic mixture with liquid circulation. A simplified drawing is shown in figure 2.3

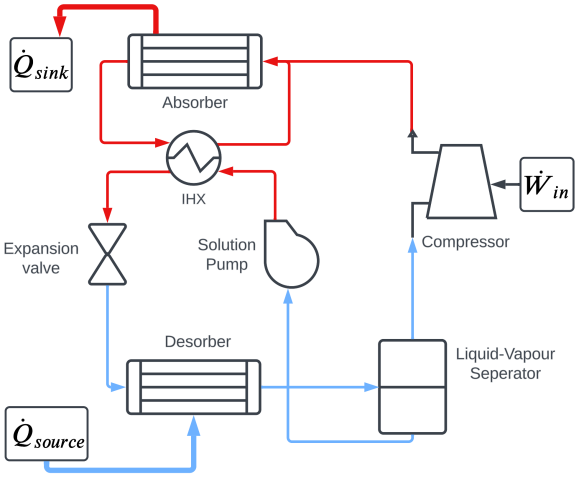

Figure 2.3: Layout HACHP, modeled after [14]

In an ammonia-water HACHP the heat from the source is used to heat a zeotropic mixture in the desorber. This mixture will not be totally evaporated and will go to the liquid-vapor separator. The ammonia rich vapor gets compressed using a compressor while the water rich liquid gets pumped towards the absorber. An internal heat exchanger is used to pre-heat the liquid before entering the absorber. In the absorber the heat is released to the heat sink.

Research

A lot of research has been done on the performance of HACHP. In 1993 Zigler and Riesch compared the performance of experimental and existing absorption cycles with vapor compression in various use-cases [13]. They found that using an absorption cycle had the benefit of being more flexible than conventional cycles. The HACHP also reached $150\,^{\circ}$C at a reasonable 20 bar of pressure.

In 1997 Brunin et al. investigated the working domain of HACHP [15]. One of the findings was that it is possible to fit sink temperatures between 100 and 140 by varying ammonia concentration from 0.45 to 0.25.

In 2014 Jensen investigated the use of HACHP for high temperature applications [16]. Simulations were run with standard heat pump components rated for 28 bar, with high pressure NH_3 components rated for 52 bar and transcritical CO_2 components rated for 140 bar. It was found that compressor discharge temperature and pressure ratio were the main limitations. To reach heat sink temperatures of $150\,^{\circ}$C or $175\,^{\circ}$C the compressor of transcritical CO_2 specification should be adapted to withstand high compressor discharge temperatures of up to $250\,^{\circ}$C. NH_3 equipment was sufficient to reach heat sink temperatures of $125\,^{\circ}$C.

In 2015 Jensen followed up this research with a technical and economic analysis on the working domain of HACHP [9]. In this analysis it was found that HACHP is a preferable technology for applications where higher temperature lifts and higher heat sink temperatures are required. Concluding that HACHP shows economic benefit for all applications above $80\,^{\circ}$C.

In 2015 Bor et al. investigated various technologies for low grade waste heat recovery [17]. The main benefit of HACHP is the ability to match temperature glide in the absorber and desorber with the temperature gradient of the waste heat stream. The ability to use working fluids with 0 GWP is also a large advantage. The oil that is necessary to lubricate the compressor will accumulate on the heat exchangers reducing system performance over time.

In 2021 Qing et al. investigated the potential of a HACHP which is constrained to a maximum pressure of 50 bar and a maximum compressor discharge temperature of $180\,^{\circ}$C [18]. A numerical model was developed in MATLAB. This model was validated using data from the research of Jensen and yielded similar results. Three kind of two-stage HACHP cycles were compared to the single-stage HACHP cycle. Heat recovery, liquid injection and a flash tank intercooler were compared as cycle optimizations. It

was concluded that two-stage solutions are required to reach a temperature lift of $40\,^{\circ}$C. All of the cycle optimizations seem to be feasible.

To summarize an overview of the advantages and limitations of HACHP will be given:

Advantages

- Lower pressure compared to VCHP
- Working fluids with low GWP and ODP are commonly used
- When using two-stage cycles high temperatures lifts can be obtained
- More flexibility compared to VCHP
- Ability to match temperature glide with temperature glide of heat source/sink
- Well researched and applied technology

Limitations

- Compressor discharge temperature is limited due to lubrication oil degradation
- Need for two-stage cycle to be viable for high temperature lifts
- More equipment needed compared to VCHP increasing cost

2.3. Compression resorption heat pump with wet compression

The compression resorption heat pumps with wet compression will be named CRHP in the rest of this paper. Using wet compression to improve CRHP performance has been investigated since the last part of the last century. As explained in section 2.2 the main limitation of HACHP is the ability to reach high sink temperature due to lubrication problems in the compressor. Wet compression is a potential solution for this problem as it does two things to eliminate this problem. First it is able to operate without lubrication oil, eliminating the degradation of the oil and the oil build-up on surfaces in the heat exchangers. Second the presence of liquid in the compressor limits the superheating by evaporative cooling. First the cycle will be explained. After that the research on wet compression will be analysed and the advantages and limitations will be identified.

Cycle

The CRHP cycle can be seen in figure 2.4. The cycle is similar to the VCHP cycle in figure 1.3. The main difference is the zeotropic mixture that is used as a working fluid as well as that the working fluid does not completely evaporate at the desorber. The compressor has to be able to compress the liquid-vapor mixture.

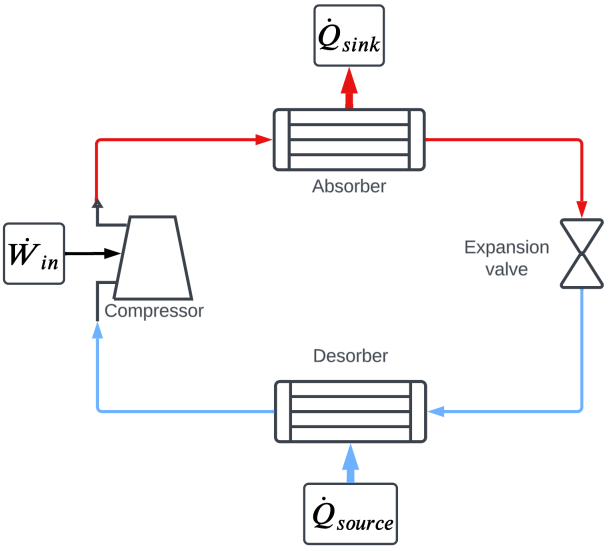

Figure 2.4: Layout CRHP

In figure 2.5 the T-s diagram of a CRHP is shown. It can be clearly seen that the absorption and desorption are not isothermal. It is also visible that the whole cycle takes place in the vapor-liquid regime.

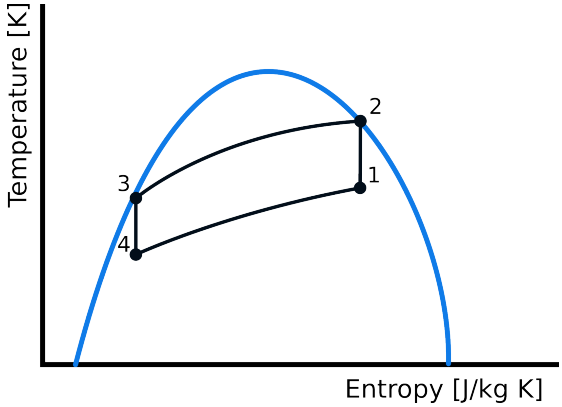

Figure 2.5: T-s diagram CRHP [19]

Research

In 1991 Bergmann and Hivessy build a pilot plant using a CRHP with wet compression [20]. In this plant the amount of liquid to enter the compressor could be varied. Smoother and more silent operation compared to dry compression was noticed. Problems with sealing and reliability were reported. The wet compression was successful in reducing the discharge temperature. Once a suitable compressor is developed the operation of a CRHP was deemed not considerably more intricate than a conventional heat pump.

In 1998 Itard reviewed the use of wet compression to enhance heat pump performance [21]. First the wet and dry cycles were compared. Assuming equal efficiencies it was concluded that for pure refrigerants wet compression may deliver a higher COP, for mixtures there is always an improvement. A model was developed to simulate the performance of a ammonia-water CRHP using wet compression. Finally a heat pump test plant was built using a liquid-ring compressor. The isentropic efficiency of the compressor was low (below 10 %). It was concluded that at the optimal concentration the main losses arise in the compressor. It was shown that a wet compressor with an isentropic efficiency of at least 0.75 should be used. A performance increase of 14 % on average was estimated compared to HACHP.

In 2003 Zaytsev investigated the design of a compressor suitable for two-phase compression [22]. Different compressor types were reviewed and it was concluded that the twin screw compressor was most suitable. This was due to the tolerance for liquid carryover, efficiency and lubrication. A computer simulation model was developed, which will be further explained in section 2.4. The model was able to quantify the irreversibilities, it was found that internal leakage flows have the largest influence on the isentropic efficiency of the compressor. It is mentioned that, while designing a compressor for a heat pump, not only the isentropic efficiency should be considered but also the COP of the plant. Higher injection flow can increase the efficiency but deliver a lower COP. A prototype compressor was designed. This was based on a water injected air twin-screw compressor which has been modified to be used in a ammonia-water CRHP. The compressor did have an isentropic efficiency of less than 10 %. To improve this it is recommended to reduce the amount of liquid in the compressor suction chamber and instead inject it in the compressor cavity where the compression has just started. More information about the temperature distribution in the compressor housing and rotors would allow for better clearance design and improve the compressor efficiency.

In 2006 Infante Ferreira et al. modified the model and experimental setup of Zaytsev [23]. By moving the liquid injection location from the suction plenum to the start of the compression the isentropic efficiency went from 5 % to 50 % in the model and from 10 % to 35 % in the experiments. The difference in efficiency was attributed to the difference in the amount of injected liquid between the model and the experiments.

In 2015 van de Bor et al. investigated the use of heat pumps and power cycles for low grade waste heat recovery [17]. In the calculations the isentropic efficiency of wet compression was assumed to be 70%. At 70% isentropic efficiency CRHP outperforms HACHP and TCHP in terms of performance. It was

noted that dry compression was able to deliver larger increases in water temperature but this came at the cost of higher compressor discharge temperatures which may not be realistic.

In 2020 Gudjonsdottir investigated the potential of wet compression in CRHP [24]. First the potential of operating with $NH_3 - CO_2 - H_2O$ instead of $NH_3 - H_2O$ was investigated. For small temperature glides $NH_3 - CO_2 - H_2O$ showed significant performance benifits, however for larger temperature glides these benefits disappeared.

In 2020 Kothari performed experiments using an oil free twin screw compressor [25]. This experimental setup was build to validate the model that was developed by Guðmundsdóttir [26]. This model uses the governing equations, compressor port properties and leakage paths developed by Zaytsev [22] and Tang [27]. The experimental setup is the same that will be used for this research. The setup is limited by a maximum temperature of $100\,°$C for the cooling water in the absorber, this means that the compressor discharge temperature has to be kept below $120\,°$C. The results were analyzed using both a homogeneous and a heterogeneous calculation scheme. This is further analysed in section 2.4.1. A difference between the model and the experimental setup of 23% in isentropic efficiency and 38% in volumetric efficiency was observed. At the highest an experimental isentropic efficiency of 44% was observed using a homogeneous calculating scheme and 75% using a heterogeneous calculating scheme.

In 2023 Brancaccio further developed the model worked on by Bommel, Guðmundsdóttir and Kothari [28][26][25][29]. The model was compared to the data achieved in the experiments of Kothari. The compressor model was integrated with three additional models: the input data model, the discharge pipe data model and the cycle model. The input data model was build to account for the not negligible gap seal flow which was approached using the nozzle flow equation which was proposed by Infante Ferreira et al. [30]. The discharge pipe data model was to simulate the heat transfer between liquid and vapor in the pipe after the compressor discharge. The cycle model was used to calculate the thermodynamic states along the cycle and the COP of the system. With these modifications, the model and experimental data align much better with a mean error of 4% at 10320 rpm, 6.5% at 12910 rpm and 10.5% at 14205 rpm. Using this, computational experimentation was performed. This was used to determine the optimum operating conditions to maximise performance. For optimal performance, the pressure ratio should be around the design pressure ratio of 3, the gap seal flow should be as low as is technically possible and the inlet vapor quality should be around 90%.

To summarize a overview of the advantages and limitations of CRHP will be given

Advantages

- High COP compared to VCHP and HACHP
- Working fluid can be used for lubrication eliminating problems with oil in the system
- The liquid in the compressor cools down the compressor limiting superheating
- Once suitable compressors exist the CRHP is not that more intricate compared to a conventional heat pump
- Ability to match temperature glide with temperature glide of heat source/sink

Limitations

- An isentropic efficiency of about 70% should be reached in order to be commercial viable
- No commercial solutions available at the time, limited data about reliability

2.4. Wet compressor

In the previous section it became clear that while CRHP shows great potential for high temperature heat pump applications a suitable compressor is necessary. In the research papers the isentropic efficiencies have been mentioned. Isentropic efficiency can be calculated by equation 2.1. Here state 1 is at the compressor inlet and state 2 is at the compressor outlet. Isentropic efficiency is the ratio between the amount of work that would have to be done if the compression were to be isentropic (without irreversibilities) and the the amount of work that it actually took.

$$\eta_{is} = \frac{h_{2,is} - h_1}{h_2 - h_1} \tag{2.1}$$

In figure 2.6 the difference between an isentropic and a real compression can be seen in a T-s diagram.

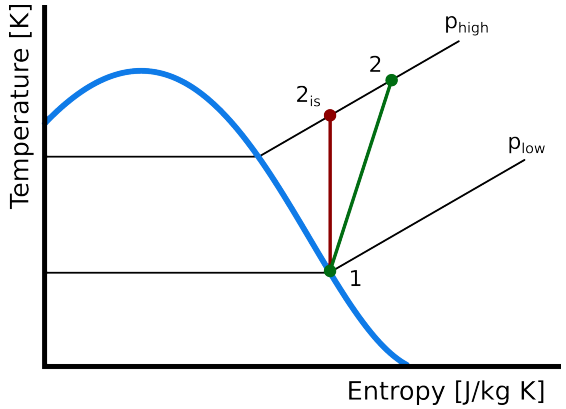

Figure 2.6: T-s diagram with isentropic and real compression

As mentioned in the previous chapter an isentropic efficiency of 70% has been identified to make wet compression feasible. For dry lubricated screw compressors isentropic efficiencies of 85% have been reached [31].

Compressors technologies
Different kind of technologies have been evaluated and tried. In 1998 Itard used a liquid ring compressor [21]. This was because there were no small scale ammonia-water screw compressors available that could work with wet compression. The liquid ring compressor did not meet the design values.

In 2003 Zaytsev did a comparison between different compressor techniques for wet compression [22]. The design requirements were:

- Large enough suction flow capacity (up to $700\,\mathrm{m}^3/\mathrm{h}$)
- Pressure ratio of 6 to 8
- Isentropic efficiency of 0.75 or more
- Oil free lubrication
- Wet compression compatibility

At the end of the comparison reciprocating, twin screw and single screw compressors seemed to meet the requirements. The single screw compressor was eliminated because small size single screw compressors were not widely available. To decide between reciprocating and twin screw compressors a simulation was was done for various industrial and urban applications. Based on these results it was decided that twin screw compressors would be more suitable for CRHP.

In 2019 Gudjonsdottir et al. investigated a wet compression model for entropy production minimization [32]. In this paper it was concluded that it is possible for a twin screw compressor to reach an isentropic efficiency higher than 70%. To obtain this the following conditions must be satisfied:

- Clearance sizes should be limited to $50\,\mu\mathrm{m}$
- Rotational speed should be above $10\,000\,\mathrm{rpm}$
- Ammonia-water concentration should be maintained in the range 30 to 40 wt.%
- The vapor quality at inlet should be in the range 0.5 to 0.7
- Under and over-compression should be avoided

The proposed compressor is using no injection in the compression chamber but into the vapor line instead.

In 2023 Ahrens et al. performed a numerical investigation of an oil-free liquid injected screw compressor [33]. In this study the liquid of a HACHP was injected in the compressor. By injecting the liquid in multiple places in the compression phase the superheating could be eliminated. The assumption was made that the working fluid exhibited homogeneous behaviour which at least for injection in the vapor line turned out to not agree with experimental results [30].

2.4.1. Modelling

As shown in the previous section the modelling of the compression process has been of great interest. In this section the governing equations used in modelling the compressor will be explained. A distinction will be made between the homogeneous approach where the liquid and vapor are in equilibrium and the heterogeneous approach where the liquid and vapor are not in equilibrium and have to be considered separately. In the modelling of screw compressors the cavity properties are calculated as a function of the turning angle of the male rotor ϕ. The three conservation equations will be shown for the homogeneous and heterogeneous approach. The formulations are taken from Zaytsev [22].

First of all it is important to consider the control volume. In a twin-screw compressor the control volume is the volume of one cavity between the male and female rotor. To obtain the cavity volume as a function of the rotor angle a geometric model needs to be made.

homogeneous approach

Because the compressor that is modelled compresses a zeotropic mixture three conservation equations should be considered:

- The conservation of mass
- The conservation of the mass of one of the components, in this case ammonia
- The conservation of energy

The conservation of mass is formulated in equation 2.2

$$dm = \sum_{k=1}^{l} dm_{in.k} - \sum_{k=1}^{n} dm_{out.k} \tag{2.2}$$

The conservation of the mass of ammonia is formulated in equation 2.3

$$d(mX_T) = \sum_{k=1}^{l} X_{Tin.k} dm_{in.k} - X_T \sum_{k=1}^{l} dm_{out.k} \tag{2.3}$$

The conservation of the energy of a control volume is given by equation 2.4

$$\delta Q + \sum_{k=1}^{l} h_{in.k} dm_{in.k} - h \sum_{k=1}^{n} dm_{out.k} = dH - V dp \tag{2.4}$$

In these conservation equation the following is considered:

- The flow through the suction, discharge, leakage paths and potential injection ports
- The volume change due to rotation of the rotors
- The heat exchange between the mixture an the compressor surface

These relations can be reformulated and differentiated to get expressions for $\frac{dp}{d\phi_1}$, $\frac{dX_T}{d\phi_1}$ and $\frac{dT}{d\phi_1}$. The mass, ammonia mass and energy conservation respectively

heterogeneous approach

For the heterogeneous approach it is assumed that the liquid and vapor phase are not in equilibrium but instead the temperature and concentration can differ from the values in equilibrium condition. This means that both phases have to be evaluated with separate sets of governing equations. This results in the following set of equations:

$$dm_V = \sum_{k=1}^{l} dm_{Vin.k} - \sum_{k=1}^{n} dm_{Vout.k} + dm_{ev} \tag{2.5}$$

$$\delta Q_{SV} - \delta Q_{VL} + \sum_{k=1}^{l} h_{Vin.k} dm_{Vin.k} - h_V \sum_{k=1}^{n} dm_{Vout.k} + h_{evap} dm_{ev} = dH_V - V_V dp \tag{2.6}$$

$$d(m_V X_V) = \sum_{k=1}^{l} X_{Vin.k} dm_{Vin.k} - X_V \sum_{k=1}^{n} dm_{Vout.k} + dm_{NH_3 evap} \tag{2.7}$$

$$dm_L = \sum_{k=1}^{l} dm_{Lin.k} - \sum_{k=1}^{n} dm_{Lout.k} - dm_{ev} \tag{2.8}$$

$$\delta Q_{SL} - \delta Q_{VL} + \sum_{k=1}^{l} h_{Lin.k} dm_{Lin.k} - h_L \sum_{k=1}^{n} dm_{Lout.k} + h_{evap} dm_{evap} = dH_L - V_L dp \tag{2.9}$$

$$d(m_L X_L) = \sum_{k=1}^{l} X_{Lin.k} dm_{Lin.k} - X_L \sum_{k=1}^{n} dm_{Lout.k} - dm_{NH_3 evap} \tag{2.10}$$

Here equation 2.5 is the mass conservation equation for the gas phase, equation 2.6 is the energy conservation equation for the gas phase, equation 2.7 is the ammonia conservation equation of the gas phase. For the liquid phase equation 2.8 is the mass conservation equation, equation 2.9 is the energy conservation equation and equation 2.10 is the ammonia conservation equation for the liquid phase. These relations can be reformulated and differentiated to get expressions for $\frac{dp}{d\phi_1}, \frac{dT_V}{d\phi_1}, \frac{dX_V}{d\phi_1}, \frac{dV_V}{d\phi_1}, \frac{dV_L}{d\phi_1}, \frac{dT_L}{d\phi_1}$ and $\frac{dX_l}{d\phi_1}$.

It is evident that solving the model for the heterogeneous approach is more involving and computational demanding. However, because of the very short residence times (0.001 s) in compressors it might be the more appropriate. In order to correctly assume a homogeneous model the droplet size has to be below 100 µm [34].

2.5. Other technologies

Other technologies have been used to recover low grade waste heat, in this section the Organic Rankine cycle and the transcritical vapor compression cycle will be evaluated for their potential to upgrade low level waste heat.

2.5.1. Organic Rankine cycle

The Organic Rankine cycle (ORC) is a heat engine that uses a Organic working fluid other than water. By using a working fluid with a lower boiling point compared to water the Rankine cycle can be used to recover low grade waste heat. In a heat engine heat is used to generate work. This gives the following following equation for the COP:

$$COP = \frac{\dot{W}_{turb} - \dot{W}_{pump}}{\dot{Q}_{in}} \tag{2.11}$$

In this case the COP is equal to the efficiency, meaning that it can not exceed 100 %.

Cycle

In figure 2.7 a layout of an ORC is shown. In an ORC heat is used to heat an organic working fluid in the evaporator, using a turbine vapor is expanded and work is extracted. The low pressure vapor is condensed and liquid gets pumped using a solution pump.

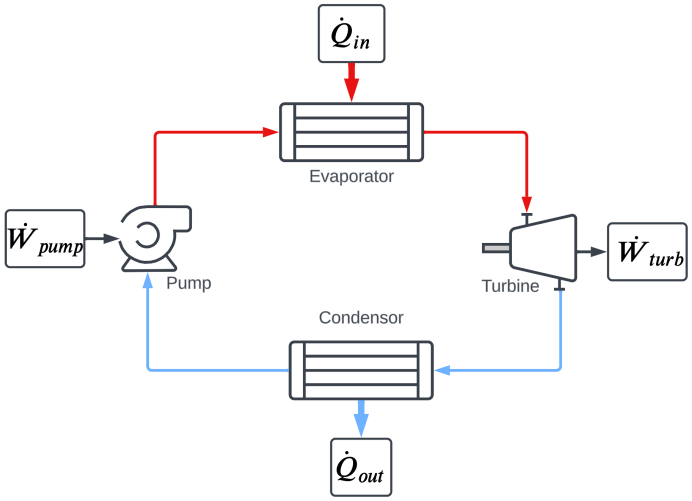

Figure 2.7: Layout ORC [35]

Applicability
In 2015 van de Bor et al. concluded ORC needs waste heat temperatures of $130\,^{\circ}$C or higher to be competitive with heat pump cycles [17]. This is mainly due to the low efficiencies of heat engines at low temperature lifts. Araya et al. concluded that for low temperature waste heat of $40\,^{\circ}$C to $80\,^{\circ}$C an efficiency of only 5% was obtained [36] . As long as upgraded waste heat can be utilized heat pumps are preferable.

2.5.2. Transcritical vapor compression heat pump

The transcritical vapor compression heat pump (TCHP) is similar to the VCHP but instead of condensing a vapor a supercritical fluid is cooled.

Cycle
The layout of the TCHP is similar to the layout in figure 1.3 with a dense gas cooler instead of a condenser. In figure 2.8 the T-s diagram of a TCHP cycle is shown.

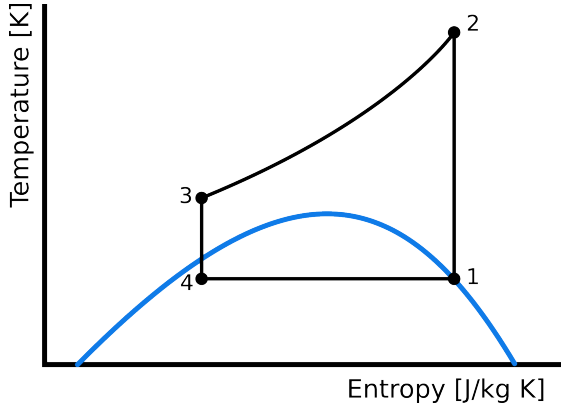

Figure 2.8: T-s diagram TCHP

The discharge of the compressor and the heat sink are in the supercritical region. This has a similar effect to the absorption process in a CRHP, because it result in a non-isothermal heat sink temperature.

Applicability
As mentioned by Jensen in 2014 TCHP equipment is rated for operating up to 140 bar [16]. This increase in operating pressure compared to the other heat pumps discussed in this chapter means that equipment cost will be higher. The TCHP has a large temperature glide at the heat sink which makes it less flexible, on the other hand it shows promising efficiencies compared to VCHP [17].

3

Research Question

The objective of this research is:

To find operational conditions to maximize the performance of a high temperature compression resorption heat pump using wet compression by developing a cycle energy balance model.

The following sub-questions were formulated in order to pursue this objective:

- What is the influence of the inlet vapor concentration on the isentropic efficiency?
- What is the influence of the gap seal flow on the isentropic efficiency?
- What is the influence of heat transfer during the compression on isentropic efficiency?
- What is the influence of rotational speed of the compressor on isentropic efficiency?

This will be achieved by using experimental data which was previously obtained by the use of an experimental set-up at the TU Delft. The sensor data will be used to develop a model that considers the total energy balance of the cycle. Limitations of the experimental setup will be identified and accounted for. At places where not enough data is available models based on empirical relations will be used to best predict the relevant properties. The results from this analysis will serve as a input for the case study where the performance of a CRHP utilizing wet compression is compared against other technologies.

4

Experiments

In this chapter the experimental setup as well as the setup limitations will be described. In order to test and validate the theoretical benefits of wet compression an experimental setup was put together in the Process and Energy Laboratory at the TU Delft. The compressor was provided by Atlas Copco and specially adapted for wet compression.

4.1. Experimental setup

In figure 4.1 a simplified drawing of the experimental setup is shown. The setup consists of the following components:

- Vapor liquid separator
- Electric tracing on vapor line
- Sub-cooler on the liquid line
- Expansion valves
- Twin screw compressor
- Plate heat exchanger absorber

The purpose of this setup is to test the performance of the twin screw compressor. This compressor has been modified by Atlas Copco to be able to run oil-free on the process side. The work that has been performed on the setup in preparation for additional tests is explained in Appendix A.

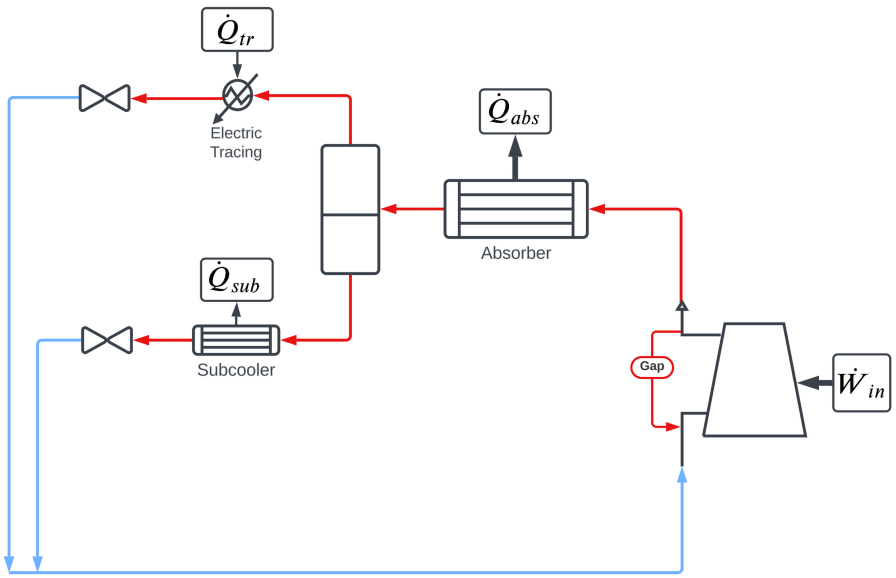

Figure 4.1: Simplified drawing of experimental setup at P&E Lab

This setup was configured in order to analyse the performance of the wet compressor. This wet compressor is designed for the use in CRHP's, this setup however is not a heat pump since it only contains an absorber and misses the desorber. The result of this is that almost all of the energy that is transferred from the compressor to the working fluids gets removed in the absorber. Following the components of the experimental setup will be briefly explained.

Vapor liquid separator
The vapor liquid separator is a larger vertical vessel which contains a large part of the total working fluid at a fixed temperature and pressure. The working fluid inside the separator is in vapor liquid equilibrium and with a two component mixture this means that the liquid and the vapor phase have a different composition. In the case of the experimental setup, the liquid phase will be mostly water, and the vapor phase will be mostly ammonia. There are exits at the top and bottom, which are connected to the vapor and liquid lines, respectively.

Electric tracing
On the vapor line, which originates from the top of the vapor liquid separator, there is an electrical tracing. These are wires with high current wrapped around the vapor line. The electrical tracing is placed to heat the working fluid to ensure that the working fluid is totally vaporized at the mass flow meter which is placed before the expansion valve.

Sub-cooler
The sub-cooler has a similar purpose as the electrical tracing. It is a plate heat exchanger placed on the liquid line in order to ensure that the working fluid that moves through the liquid mass flow meter is completely liquefied. There are thermometers and a mass flow sensor on the cooling water side to precisely calculate the amount of heat that is deducted from the working fluid.

Expansion valves
On both the liquid and the vapor line an expansion valve is placed. These expansions valves can be precisely regulated by the control software. This ensure that the properties at the compressor inlet are in a desirable range.

Twin screw compressor
The most important part of this setup is of course the wet twin screw compressor. The compressor compresses combined flow from the liquid and vapor line. The sealing and the cooling of this compressor is originated from the liquid working fluid present in the compressor. For this study there are two significant elements of the compressor that are considered. The first is the oil cooling that goes through the compressor housing and the second is the gap seal flow. The gap seal flow is a flow that goes from the high pressure side to the low pressure side and is necessary in order to seal the process side from the housing. The amount of flow over the gap seal was previously assumed to be negligible however recent analysis indicated that the flow over the gap seal is significant compared to the total compressor flow [30].

Plate heat exchanger absorber
The energy that is added to the working fluid in the compressor is taken away by the absorber. The absorber consist of two plate heat exchanger in series. In the heat exchanger part of the vapor will condense and both the vapor and the liquid will become richer in ammonia.

4.2. Experimental procedure

For this thesis the data obtained by Kothari [25] will be used. In this section the experimental procedure used to obtain and process the data will be explained.

4.2.1. Procedure

The procedure contains of four steps:

- Start up the setup
- Reach steady state
- Start data recording

- Data processing

First the setup is started and the valves, compressor and cooling water flow are adjusted until the system stabilized at the desired properties for that run. Properties that were varied were among others the pressure ratio, inlet vapor content and the inlet temperature. Once the desired values are stable the setup has reached steady state. From this moment the measurement data is logged and saved to the computer. This data is stored in .CSV files and can later be averaged and used as inputs to calculate the compressor performance.

4.3. Experimental setup limitations

The setup has a few limitations that make correctly assessing the wet compressor performance difficult. This is partly due to the heterogeneous behavior and partly due to the placement of some of the sensors. In this section the limitations of the setup will be explained. Four limitations are considered:

- The heterogeneous behavior
- The gap seal flow
- The compressor oil cooler
- Discharge side pressure drop

In this section these limitations will be explained. In chapter 5 models will be implemented to predict these limitations.

4.3.1. heterogeneous behavior

It was concluded by Infante Ferreira [30] and Brancaccio [29] that the behavior inside the compressor has to be considered heterogeneous. This means that the vapor and liquid are not necessarily in equilibrium and might have different properties. In figure 4.2 a simplified drawing of the two phases is shown. Here the vapor and liquid have different temperatures and composition but the same pressure. It has to be noted that with equal mass flows most of the volume would be taken up by the vapor. This is because the density ratio between vapor and liquid is around 900 for both water and ammonia.

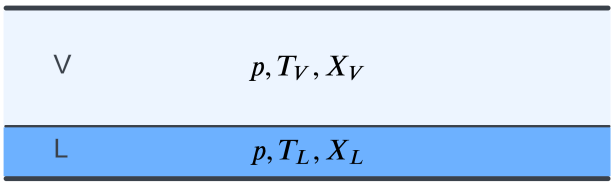

Figure 4.2: heterogeneous flow through a pipe

The mixture will always tend to go to equilibrium between the phases by transfer of heat. This means that heterogeneous behavior should only be considered at or near places where properties change quickly. In this setup that is at the expansion valves, the compressor and the compressor exit.

The temperature sensor at the exit of the compressor is in a part of the setup where the setup is still likely to be heterogeneous as shown by Brancaccio [29]. Due to this placement it is not certain which temperature is measured, that of the vapor, the liquid or something in between.

4.3.2. Gap seal flow

During past experiments using the experimental setup it became clear that there was a non negligible flow from the compressor discharge side to the compressor suction. In figure 5.9 it is illustrated how this flow moves. This is called the gap seal flow. The gap seal flow is necessary in order to create the sealing between the rotors and the fixed housing of the compressor.

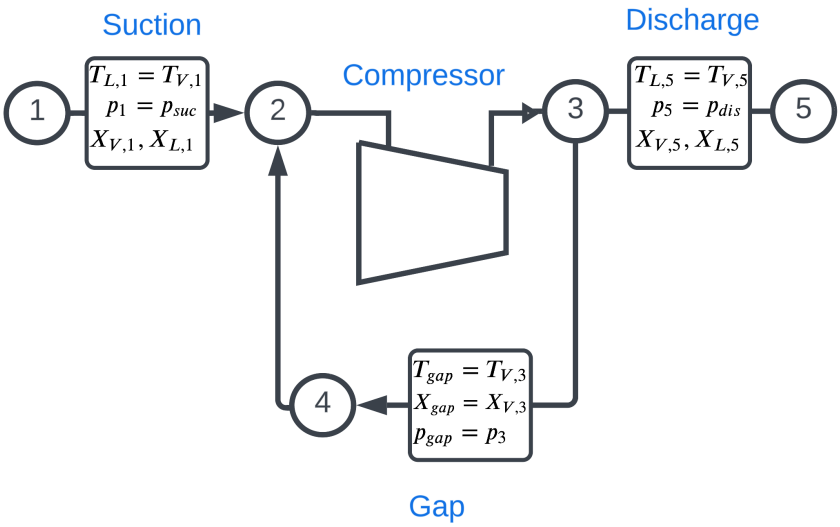

Figure 4.3: Gap seal flow compressor

The existence of the gap seal flow means that the mass flow through the compressor itself is higher compared to the mass flow in the rest of the system. This affects the calculation of the isentropic efficiency. If the gap seal flow is not taken into account the isentropic efficiency would be calculated as in equation 4.1.

$$\eta_{is,tot} = \frac{h_{5,is} - h_1}{h_5 - h_1} \tag{4.1}$$

If the isentropic efficiency of only the compressor itself is calculated we have to use equation 4.2.

$$\eta_{is,comp} = \frac{h_{3,is} - h_2}{h_3 - h_2} \tag{4.2}$$

It has to be noticed here that $\eta_{is,tot}$ is larger than $\eta_{is,comp}$. This is because the mass flow rate through the compressor is much larger because of the additional flow through the compressor.

For this setup we want to know the compressor performance both with and without the gap seal flow. The first reason for this is because it is very likely that the gap seal flow can be reduced by either redesigning the seal or by regulating the flow. The second reason is that in order to determine the operating window where this compressor has its highest efficiency the inlet properties have to be precisely determined. The properties at points 2, 3 and 4 are not measured. Moreover the conditions at these points are heterogeneous. This means that careful analysis is required in order to get a accurate indication of the performance of the wet compressor. In chapter 5 the whole wet compressor is modelled paying special attention to the gap seal flow and heterogeneous mixture. By identifying the size and properties of the gap seal flow it becomes possible to make an accurate prediction with what isentropic efficiency wet compression could be implemented.

4.3.3. Compressor oil cooler

The compressor housing is lubricated and cooled by the lubrication oil that also flows through the compressor gearbox. This oil is cooled using a plate heat exchanger and is kept below $25°$C. The oil flow through the housing will have a cooling effect on the process fluid inside and therefor the compression process will not be adiabatic. The amount of heat that is transferred from the process to the oil will be calculated and adjustments will be made in order to account for this effect on the compressor performance calculation.

4.3.4. Pressure drop

At the high pressure side of the setup the pressure is only measured at the compressor discharge. In the previous studies of the performance of the experimental setup the pressure at the separator was considered equal to the pressure at the compressor discharge. A difference in these two pressures would make the study inaccurate because the pressure and temperature data from the separator are used in order to calculate the ammonia concentrations of the liquid and vapor line originating from the separator.

5 Modelling

In this chapter the model that was developed will be explained. This model was developed in order to correctly analyse the data from the experimental setup. The model was developed partly in Matlab and partly in Aspen. The code in Matlab is used to calculate heterogeneous properties and is used as input for the Aspen model. The goal of the model is to calculate the compressor performance in a variety of conditions.

5.1. Model outline

First a model of the entire setup was made in Aspen Plus 12. This was done to quickly calculate all the properties and to have a graphical interface. This graphical interface helps to quickly view the temperatures, pressures and mass flows. Moreover it also calculates the heat flows which gives quick insight in the heat balance of the system.

The Matlab part of the model is used in order to perform the heterogeneous and heat calculations and to quickly feed the data from different runs to the Aspen model. The calculations that are performed in Matlab follow from the wet compression, heat transfer and the heterogeneous assumptions that are made.

5.1.1. Model structure

In figure 5.1 the model structure is shown. First the raw data is loaded from a CSV file. This data is converted to SI units and averaged. This averaged data is stored and can be quickly accessed. After that fluid properties are calculated as initial guesses. The simulation runs in Aspen and properties are updated from Matlab in order to iterate until the isentropic efficiency converges. During the simulation the thermodynamic properties that are related to the heterogeneous behavior are calculated and updated in each iteration. In the end the isentropic efficiency as well as the temperatures, compositions and mass flows of all the streams are calculated.

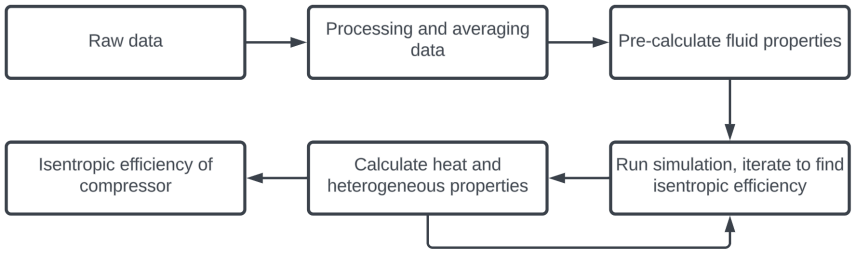

Figure 5.1: Structure of the model

For the modelling of the experimental setup a couple of assumptions are made. First the behavior of the process fluid in the compressor and between the compressor and absorber is assumed heterogeneous. This means that the liquid and vapor are not in equilibrium and heat transfer between the phases has to be considered. The rest of the setup is assumed homogeneous. The whole cycle operates at temperatures between 60 and 200 degrees Celsius.

5.2. Aspen Model

Aspen was used to create a model of the entire cycle. This was done in order to create a different way of evaluating the cycle performance that did not involve temperature measurements in heterogeneous parts of the system. First the model layout and inputs will be shown. Second the extra steps necessary in order to implement the wet compressor in Aspen are explained. This has to be done because Aspen does assume the vapor and liquid to be in equilibrium at each substream. Finally the method to determine the isentropic efficiency is explained. The model is created after the P&ID as pictured in figure 5.2. Here changes have been made to account for the wet compression. Here CW1, CW2 and CW3 are the three cooling water streams that are used. CW1 cools the absorber and makes it possible to obtain stable operation. CW2 cools the sub-cooler and ensures that the liquid stream that is measured is entirely liquid. CW3 is for the oil cooler of the compressor.

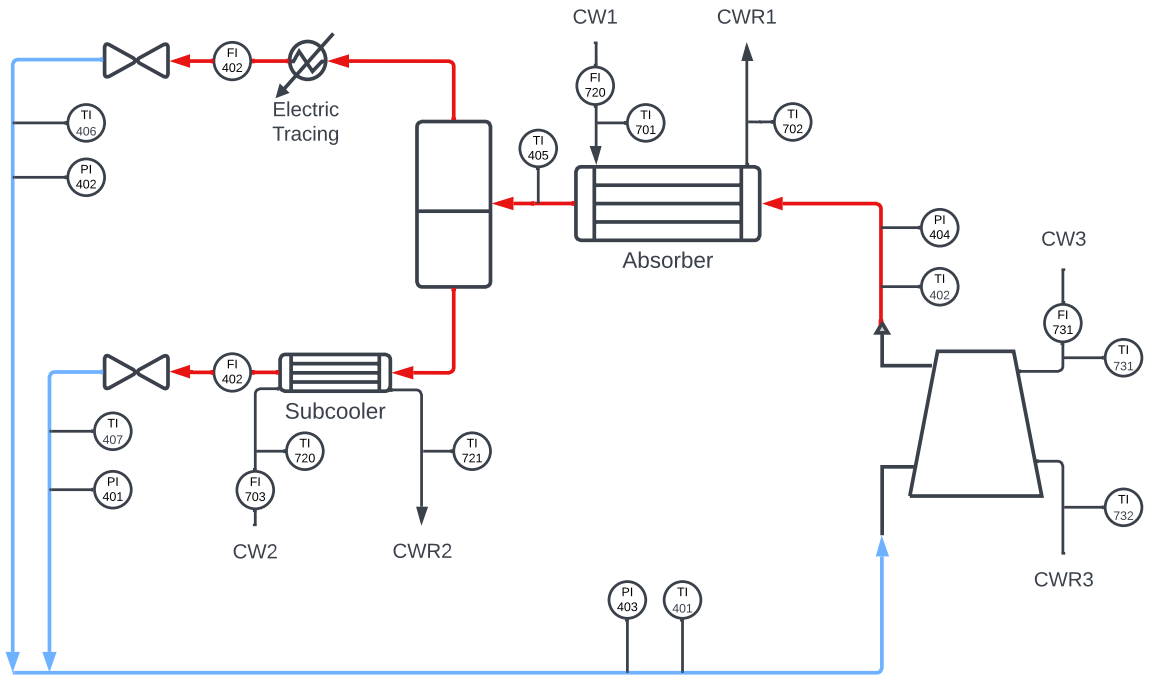

Figure 5.2: P&ID

5.2.1. Model layout

The model in Aspen looks very much like the P&ID in figure 5.2. The largest differences are that the cycle is not closed and that the wet compressor needs additional attention in order to represent the one used in the setup. In figure 5.3 the setup used in Aspen is shown. As can be seen this provides a nice graphical interface where pressures, temperatures and mass flows throughout the setup can quickly be analyzed.

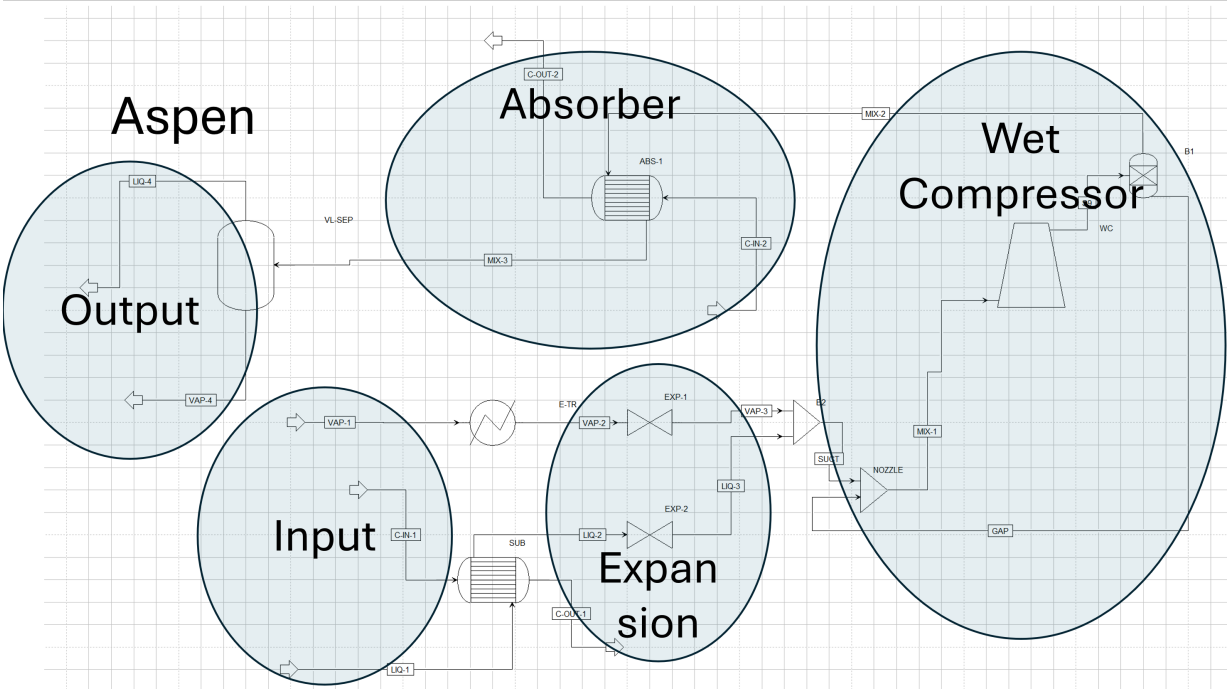

Figure 5.3: Aspen model used

This model can be roughly split into three segments, the input & expansion, the compression and the absorption & output. The expansion and input are shown in figure 5.4

5.2.2. Input and expansion

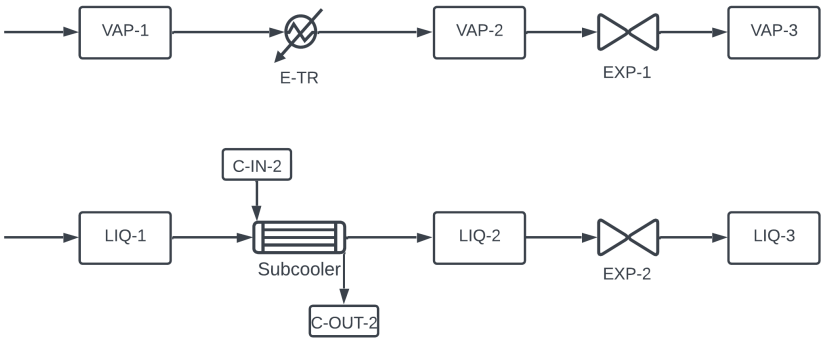

Figure 5.4: Input and expansion

The Aspen model takes the liquid and vapor stream from the separator as inputs. The compositions are calculated using refprop by:

$$X_{V_{sep}} = f(T_{405}, p_{sep}, q = 1) \tag{5.1}$$

$$X_{L_{sep}} = f(T_{405}, p_{sep}, q = 0) \tag{5.2}$$

In the first instance p_{sep} will be equal to p_{404}. Using the results from that calculation the pressure drop is calculated and this is iterated until the proper separator liquid and vapor compositions are found. For the values of the temperatures, mass flows and pressures the sensor values as shown in figure 5.2 are used unless indicated differently. Here the temperature and pressure values are directly from the sensor

data. The electric tracing heating is taken as $\dot{Q}_{tr} = 300$ W since this is what it is rated for. The sub-cooler cooling is calculating using the temperature and mass flow sensors in place using:

$$\dot{Q}_{sub} = \dot{m}_{cw,sub} \cdot c_{p,water} \cdot (T_{720} - T_{721}) \tag{5.3}$$

The expansions are both assumed isenthalpic.

5.2.3. Wet compressor

In order to emulate the wet compressor including the gap seal flow the compressor has been modelled as can be seen in figure 5.5. First the expanded vapor and liquid are mixed, this represents the place where the vapor line and liquid line of the setup connect and the liquid is injected using a nozzle. After this there is the second mixer, this is where the gap seal flow mixes with the suction flow. Here $p_{suc} = p_{403}$ and $p_{dis} = p_{404}$.

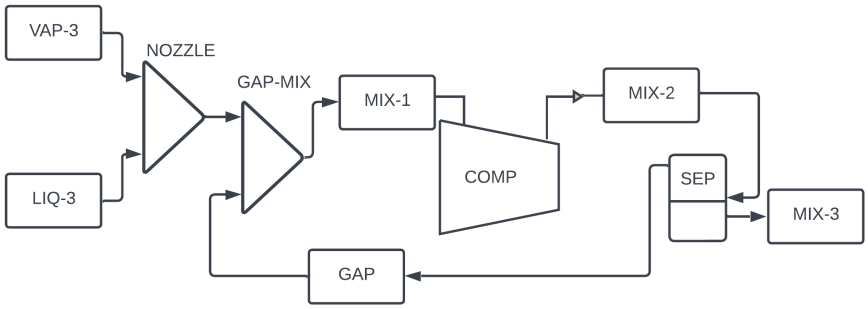

Figure 5.5: Aspen compressor model

To model the separation of the discharge flow into the gap seal flow and the mixture that goes to the absorber a separator is used. The calculation of the input parameters for the size and composition of the discharge and gap seal flow is done in Matlab and is described in section 5.3.2.

5.2.4. Absorption and output

The absorption is modelled as shown in figure 5.6. Here the absorber duty is calculated using the flow rates and temperature readings from the experimental measurements. After the absorber the vapor and liquid are separated using a separator and the cycle is considered closed when the output matches the input.

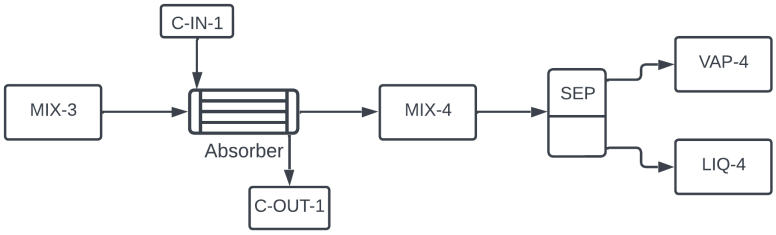

Figure 5.6: Aspen absorber and output

5.2.5. Efficiency calculations

The goal of the Aspen model is to calculate the isentropic efficiency of the cycle. In order to do that the Newton Rapson method is used to find the isentropic efficiency corresponding to a certain set of properties. This is done in the following way:

It begins with a guess for the isentropic efficiency η_{is_1}. Using this isentropic efficiency the entire cycle is run in aspen which results in a output temperature which represents the temperature in the separator $T_{sep}(\eta_{is_1})$. A small $\Delta\eta_{is} = 0.002$ is chosen. This is used to calculate $\eta_{is_{1*}}$.

$$\eta_{is_{1*}} = \eta_{is_1} + \Delta\eta_{is} \tag{5.4}$$

Using $\eta_{is_{1*}}$, T_{sep*} is calculated by running the Aspen model. This T_{sep*} allows us to calculate T'_{sep} as per equation 5.5

$$T'_{sep} = \frac{T_{sep}(\eta_{is_{n*}}) - T_{sep}(\eta_{is_n})}{\Delta\eta_{is}} \tag{5.5}$$

Using this result the isentropic efficiency can be iterated by using equation 5.6

$$\eta_{is_{n+1}} = \eta_{is_n} + \frac{T_{sep}(\eta_{is_n})}{T'_{sep}(\eta_{is_n})} \tag{5.6}$$

This is iterated untill $|T_{sep}(\eta_{is_n}) - T_{405}| < 0.001$. Where T_{405} is the temperature of the sensor placed before the separator.

5.3. Matlab Model

There are certain limitations to simply using the sensor data as mentioned in section 4.3. These limitations mainly are caused by the heterogeneous behaviour, heat transfer and wet compression. In this section the Matlab models that serve as input for the Aspen model are explained.

5.3.1. Pressure drop

In section 4.3.4 it was explained that there might be a pressure drop between the compressor discharge and the separator. In this section the procedure used to calculate this pressure drop will be explained. The pressure drop is calculated for the straight pipes, bends and contraction separately. In general pressure drop can be calculated using equation 5.7.

$$\Delta p_{tot} = \Delta p_{fr} + \Delta p_g + \Delta p_a \tag{5.7}$$

Here Δp_{fr} is the frictional pressure drop, Δp_g is the gravitational pressure drop and Δp_a is the acceleration pressure drop. In this model the gravitational pressure drop will be neglected since the separator and the pressure gauge at the discharge are roughly at the same height.

Acceleration pressure drop

The acceleration pressure drop can be calculated for the entire segment at once using equation 5.8.

$$\Delta p_a = (u_{sep}^2 \cdot \rho_{V,sep} \cdot \alpha_{sep} + u_{sep}^2 \cdot \rho_{L,sep} \cdot (1 - \alpha_{sep})) - (u_{dis}^2 \cdot \rho_{V,dis} \cdot \alpha_{dis} + u_{dis}^2 \cdot \rho_{L,dis} \cdot (1 - \alpha_{dis})) \tag{5.8}$$

Where α is the void fraction and u is the velocity of the fluid. The fluid is assumed to have simular flow speed in the liquid and vapor phase $u_V = u_L$. The vapor and liquid density values at the discharge are calculated using refprop following:

$$\rho_{V,dis} = f(T_{V,dis}, p_{dis}, X_{V,dis})$$

$$\rho_{L,dis} = f(T_{L,dis}, p_{dis}, X_{L,dis})$$

The pressure at the separator is at first taken as equal to the discharge pressure and is after that iterated to account for the property change due to the pressure change. With the pressure and temperature at the separator known the vapor fraction as well as the vapor and liquid composition are calculated.

$$X_{L,sep}, X_{V,sep}, q_{sep} = f(T_{sep}, p_{sep}, X_T)$$

With this the vapor and liquid densities are calculated.

$$\rho_{V,sep} = f(T_{V,sep}, p_{sep}, X_{V,sep})$$

$$\rho_{L,sep} = f(T_{L,sep}, p_{sep}, X_{L,sep})$$

Frictional pressure drop
The second component to the pressure drop that is considered is the frictional pressure drop. The frictional pressure drop is created due to the velocity differences throughout the cross-section of the pipe and depends on geometry, flow speed and flow composition. For the setup two kinds of frictional pressure drops are taken into account: The straight tube pressure drop and the bends pressure drop.

For the straight tube pressure drop an empirical relation developed by Garcia et al. is used [37]. In this calculation first the Fanning friction factor f_m is calculated as in equation 5.9. This coefficient is used to calculate the pressure drop as in equation 5.10.

$$f_m = 0.0925Re^{-0.2534} + \frac{13.98Re^{-0.9501} - 0.0925Re^{-0.2534}}{(1 + (\frac{Re}{293})^{4.864})^{0.1972}} \tag{5.9}$$

$$\Delta p_{str} = \frac{2 \cdot f_m \cdot L \cdot \rho_m \cdot u_m^2}{D} \tag{5.10}$$

Where ρ_m is the average density of the fluid. And u_m is the average velocity of the fluid.

For the bends the single phase pressure drop is calculated first and this pressure drop multiplied with a two phase multiplier. Using this method the bend pressure drop is calculated using equation 5.11. This relation was developed by Chisholm [38].

$$\Delta p_{bend} = \Delta p_L \cdot \Phi_L^2 \tag{5.11}$$

Where the two phase multiplier is calculated as in equation 5.12.

$$\Phi_L^2 = 1 + (\frac{\rho_L}{\rho_V} - 1) \cdot (B \cdot q \cdot (1 - q) + q^2) \tag{5.12}$$

and

$$B = 1 + \frac{2.2}{\zeta \cdot \frac{x}{D} \cdot (2 + \frac{r_{bend}}{D})} \tag{5.13}$$

Here $\frac{x}{D}$ is the equivalent length and $\frac{r_{bend}}{D}$ is the relative bend radius. For this setup $\frac{r_{bend}}{D} = 2$ which means that $\frac{x}{D} = 12$. The Darcy friction factor ζ is calculated using equation 5.14 if $2 \cdot 10^4 < Re < 2 \cdot 10^6$ and by solving equation 5.15 if $Re > 2 \cdot 10^6$.

$$\zeta = 0.0054 + \frac{0.3964}{Re^{0.3}} \tag{5.14}$$

$$\frac{1}{\sqrt{\zeta}} = -0.8 + 2log(Re_L\sqrt{\zeta}) \tag{5.15}$$

The pressure drop that results from the contraction is mainly from the increase in flow speed and not due to the friction since the angle is shallow ($\alpha < 40°$). This means that the pressure drop from the contraction is already taken into account with the calculation of the acceleration pressure drop [39].

5.3.2. Compressor model

In this section the mechanics of what happens during compression is modelled. Because equilibrium between the phases can not be assumed the local properties are of interest. First the computation of the pressure inside the compressor is explained. Second the heat transfer between the phases and to the oil is approached and calculated

For this thesis a model based on a reference compressor last adjusted by Brancaccio was used for the cavity volume and pressure distribution [28],[29]. This model is based on a reference twin screw compressor. This reference compressor was used since the exact geometries of the experimental compressor are unknown. The known properties of the experimental compressor are listed in table 5.1. For the model the geometry of the reference compressor was analyzed and scaled to match the known geometry of the experimental compressor.

Table 5.1: Geometrical properties of the experimental compressor [30]

Maximum cavity volume	$5.72 \times 10^{-5}\,\mathrm{m}^3$
Length of the compressor	$0.084\,\mathrm{m}$
Male rotor diameter	$0.084\,\mathrm{m}$
Rotational speed male rotor	$7740 - 15500$ RPM
Number of lobes on male rotor	5
Number of lobes on female rotor	6
Clearances	$0.050\,\mathrm{mm}$
Housing area	$0.0353\,\mathrm{m}^2$

The properties inside the compressor will be computed as a function of ϕ, the male rotor angle. A change of rotation in the male rotor angle $d\phi$ corresponds with area dA over which heat and mass transfer calculations will be performed. In order to relate the male rotor angle with the corresponding compressor housing area the cavity volume is used. Heat transfer area per degree as a function of the male rotor angle is shown in figure 5.7. Using this volume distribution the area dA^i is calculated using equation 5.16. Here $V_{cav,m}$ is the average cavity volume and A_{ch} is the compressor housing area. Here it is assumed that all the liquid is deposited at the compressor housing wall due to the centrifugal forces from the high rotation speed of the rotors. This drastically decreases the heat contact area compared to a vapor liquid mixture where liquid droplets are evenly distributed.

$$dA^i = A_{ch} \cdot \frac{d\phi}{852} \cdot \frac{V^i_{cav}}{V_{cav,m}} \tag{5.16}$$

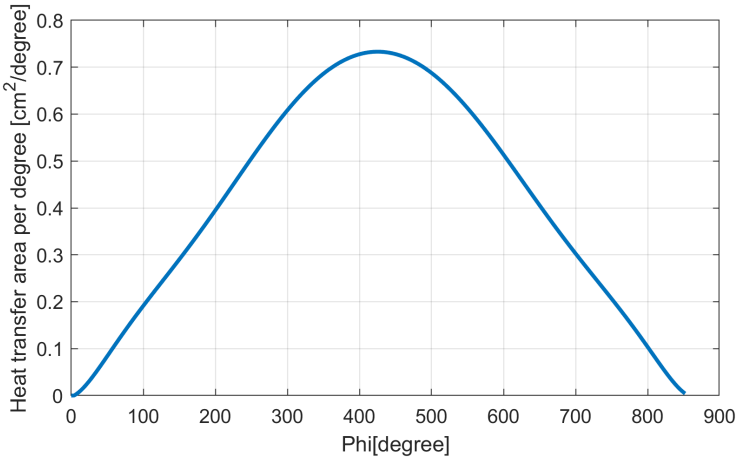

Figure 5.7: Heat transfer area per degree as a function of male rotation angle

Pressure distribution

For the pressure distribution inside the compressor it is assumed that the pressure profile throughout the compressor has an identical shape regardless of the precise compressor conditions. This was deemed reasonable since the pressure ratio typically only varies between 2.5 and 3.5. A curve fit was applied to the pressure. The pressure is described by equation 5.17.

$$\begin{aligned} p &= p_{suc} && 0 < \phi < 480 \\ p &= (p_{dis} - p_{suc}) \cdot (8.94 \cdot 10^{-8}\phi^3 - 1.40 \cdot 10^{-4}\phi^2 + 7.44 \cdot 10^{-2}\phi - 13.341) + p_{suc} && 480 \leq \phi < 720 \\ p &= p_{dis} && 720 \leq \phi \leq 852 \end{aligned} \tag{5.17}$$

This pressure distribution is shown in figure 5.8. It can be seen that the compression only happens in a small portion of the compressor. Using this relation allows for faster computation of the pressure profile and therefor heat transfer inside the compressor.

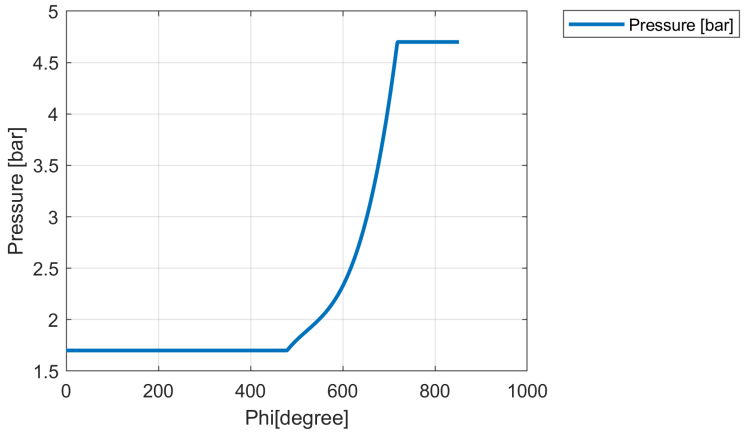

Figure 5.8: Pressure distribution inside the compressor

Gap seal flow

The gap seal flow is calculated using the nozzle equation as shown in equation 5.18. To calculate the properties of the gap seal flow the composition of the discharge vapor flow is used. The value of C_{gap} is the flow coefficient which was estimated by Infante Ferreira [30]. This flow coefficient was calculated by analyzing the energy balance of the compression and based on a heterogeneous calculation scheme. For the heterogeneous case this resulted in $C_{gap} = 0.0006$. For the gap seal flow the properties of the vapor outlet stream are considered. This is because the gap seal tube is connected at a right angle compared to the discharge flow direction. The liquid droplets have a higher momentum compared to the vapor stream and are less likely to make a large direction change. It has to be noted that the analysis by Infante Ferreira makes use of different assumptions regarding the compressor outlet conditions. It assumes that the temperature measured at the discharge is the liquid temperature. This analysis does not utilize the temperature at the compressor discharge but instead calculates back from the conditions after the absorber utilizing the absorber duty.

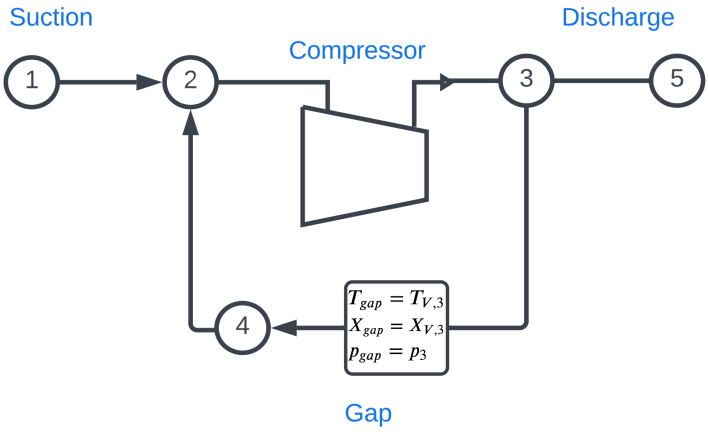

Figure 5.9: Gap seal flow compressor

$$\dot{m}_{gap} = C_{gap} \cdot \sqrt{2 \cdot \rho_{gap} \cdot (p_3 - p_2))} \tag{5.18}$$

The gap seal flow is calculated for each iteration in order to accurately calculate the compressor suction composition. At the compressor inlet the fluid properties have to be calculated by combining the gap seal flow and the flow from the liquid and vapor line. In order to do this first the total enthalpy and total ammonia

concentration are calculated using equation 5.19 and equation 5.20 respectively.

$$h_{2,T} = \frac{\dot{m}_1 \cdot h_{1,T} + \dot{m}_{gap} \cdot h_{3,V}}{\dot{m}_2} \tag{5.19}$$

$$X_{2,T} = \frac{\dot{m}_1 \cdot X_{1,T} + \dot{m}_4 \cdot X_{3,V}}{\dot{m}_2} \tag{5.20}$$

Assuming that the flows are homogeneous at the compressor suction the vapor quality and phase compositions can be determined using equation 5.21. The liquid and vapor flow are calculated using equation 5.22 and equation 5.23 respectively.

$$q_2, X_{2,L}, X_{2,V} = f(p_2, h_{2,T}, X_{2,T}) \tag{5.21}$$

$$\dot{m}_{2,L} = (1 - q_2) \cdot \dot{m}_2 \tag{5.22}$$

$$\dot{m}_{2,V} = q_2 \cdot \dot{m}_2 \tag{5.23}$$

Heat transfer
In this section the heat transfer inside the compressor will be investigated. When a vapor gets compressed work is done to the vapor which results in a temperature increase. The liquid is almost completely incompressible which means that it does not experience the same temperature rise due to compression. Inside the twin screw compressor the mixture gets compressed rapidly which means that the vapor will have a different temperature compared to the liquid and the two phases will exchange heat.

Around the compressor there is a lubrication oil flow from the same oil as in the compressor gearbox. This oil is kept below $30°$C using a plate heat exchanger. Because this oil flow is relatively cold and close to the compression chamber it is likely that this heat loss is not negligible and should be accounted for. In figure 5.10 a cross-section of the compressor is sown. Here the layers are not to scale but are in the right order. With a superheating vapor in the middle and the cold oil flowing through the compressor housing. The vapor and liquid layer need to be considered separately in order to accurately determine their composition and temperature.

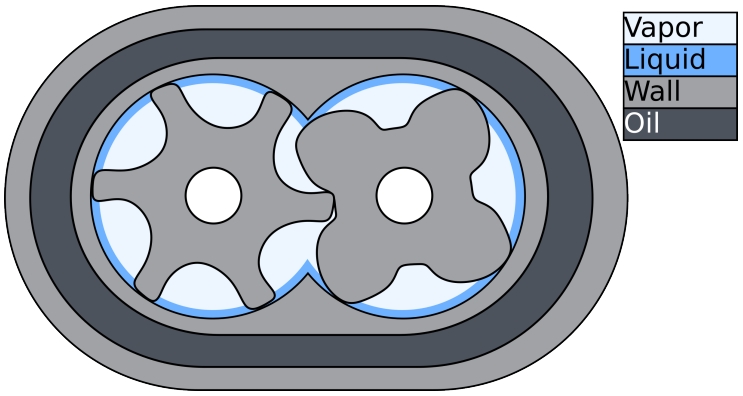

Figure 5.10: Schematic drawing of the compressor

In the rest of this section the heat transfer from vapor to liquid $\dot{Q}_{VL}$ and the heat transfer from liquid to oil $\dot{Q}_{LO}$ will be approached by the use of empirical relations for heat transfer.

Vapor to liquid
At the vapor liquid interface in the compressor there is heat transfer from a hot vapor to a colder liquid. The mixture enters the compressor in equilibrium inside the compressor the pressure rises which results in heating of the vapor. This results in boiling at the liquid vapor interface driven by the temperature difference

between the phases. This case is the most similar to film boiling. A phenomena in pipe flow where there is no contact between the pipe walls and the fluid, and the heat transfer is limited by the slower heat transfer of a liquid vapor interface.

The empirical relation that was used is developed by Wallis and Collier [40]. This relation predicts the heat transfer from a turbulent vapor to a liquid as described in equation 5.24

$$h_{VL} = 0.056 \cdot \frac{k_V}{x} \cdot Re_V^{0.2} (Pr_V Gr_V)^{1/3} \tag{5.24}$$

Here x is the the distance from the suction port. The Reynolds number is calculated by equation 5.25, he Prandtl number is calculated by equation 5.26 and the Grashof number is calculated using equation 5.27. In order to calculate the vapor flow speed it is assumed that the vapor and liquid velocity are equal.

$$Re_V = \frac{x \cdot u_V \cdot \rho_V}{\mu_V} \tag{5.25}$$

$$Pr_V = \frac{c_{p,V} \cdot \mu_V}{k_V} \tag{5.26}$$

$$Gr_V = \frac{x^3 \cdot g \cdot \rho_V \cdot (\rho_L - \rho_V)}{\mu_V^2} \tag{5.27}$$

Liquid to oil

Another important heat loss to take into account is the heat that is removed by the oil that flows through the compressor housing. To calculate this heat loss three thermal resistances are taken into account. First the thermal resistance from the liquid to the compressor housing R_{LW}. Second the thermal resistance from the conduction through the steel wall R_W. Finally the thermal resistance from the wall to the oil R_{WO}. These will be combined as shown in equation 5.28. Here U_{LO} is the total thermal conductance from the liquid to the oil.

$$U_{LO} = \frac{1}{R_{LW} + R_W + R_{WO}} \tag{5.28}$$

Where R_{LW} is calculated using equation 5.29. Here A_1 is related to the compressor housing area A_{ch}. When considering R_{LW}^i corresponding with a small rotation from the male rotor A_1 is equal to dA^i.

$$R_{LW} = \frac{1}{h_{LW} \cdot A_1} \tag{5.29}$$

The thermal wall resistance is calculated using equation 5.30. This is the thermal resistance for a concentric cylinder. Here the inner radius is calculated using equation 5.31. Here it is assumed that the compressor is a cylinder with an equal cross section as the wet compressor used. The outer radius is calculated using equation 5.32. Here is the compressor housing thickness t_{ch} assumed to be 0.01 m thick. It has to be noted that for a reasonable wall thickness range the heat transfer coefficient is high so the lack of knowledge of the exact geometry of the compressor will not influence the total heat transfer coefficient to much. When considering R_W^i corresponding with a small rotation of the male rotor L is taken as $L_{ch} \cdot \frac{dA^i}{A_{ch}}$.

$$R_W = \frac{ln(r_2/r_1)}{2 \cdot \pi \cdot k_{steel} \cdot L} \tag{5.30}$$

$$r_1 = \frac{\sqrt{A_{cr}}}{\pi} \tag{5.31}$$

$$r_2 = r_1 + t_{ch} \tag{5.32}$$

The final thermal resistance R_{WO} is calculated using equation 5.33. As can be seen in figure 5.10 the oil contacts the metal housing at multiple points. The heat from the compression chamber will conduct

through the entire housing and by thereby transfer heat over a larger area than only the outside of the compression chamber. To account for this the area A_2 is taken as $A_2 = 1.5 \cdot A_1$.

$$R_{WO} = \frac{1}{h_{LO} \cdot A_2} \tag{5.33}$$

The heat transfer coefficients from the fluids to the wall will be calculated using the Dittus Boelter equation, as introduced by McAdams [41] and is shown in equation 5.34 and equation 5.35.

$$Nu_{LW} = 0.023 \cdot Re_{LW}^{0.8} \cdot Pr_{LW}^{n} \tag{5.34}$$

$$Nu_{WO} = 0.023 \cdot Re_{WO}^{0.8} \cdot Pr_{WO}^{n} \tag{5.35}$$

Here n is equal to 0.4 for a fluid being heated and equal to 0.3 for a fluid being cooled. This means that for Nu_{LW}, $n = 0.3$ and for Nu_{WO}, $n = 0.4$. Since the liquid is expected not to boil at the wall interface and there is no total evaporation expected it is assumed that at the liquid-wall interface the Dittus Boelter equation gives an accurate assumption of the heat transfer. For the Reynolds number the characteristic length is taken as the length of the compressor L this results in the Reynolds number calculated in equation 5.36 and equation 5.37. For the Prandtl number the liquid and oil properties are considered as shown in equation 5.38 and equation 5.39. For the oil case the oil properties as shown in table 5.2 are taken. The oil flow speed is estimated at $1 \frac{m}{s}$.

$$Re_{LW} = \frac{L \cdot u_L \cdot \rho_L}{\mu_L} \tag{5.36}$$

$$Re_{WO} = \frac{L \cdot u_O \cdot \rho_O}{\mu_O} \tag{5.37}$$

$$Pr_{LW} = \frac{c_{p,L} \cdot \mu_L}{k_L} \tag{5.38}$$

$$Pr_{WO} = \frac{c_{p,O} \cdot \mu_O}{k_O} \tag{5.39}$$

Finally the heat transfer coefficients are calculated using equation 5.40 and equation 5.41.

$$h_{LW} = \frac{Nu_{LW} \cdot k_L}{L} \tag{5.40}$$

$$h_{WO} = \frac{Nu_{WO} \cdot k_O}{L} \tag{5.41}$$

The assumed wall and oil properties are depicted in table 5.2.

Table 5.2: Fluid properties of lubrication oil and compressor housing [42],[43],[44],[45]

Heat capacity $c_{p,O}$	Viscosity μ_O	Thermal conductivity k_O,k_{steel}	Density ρ_O	Flow speed u_O
$2000\,\mathrm{J/(kg \cdot K)}$	$0.02\,\mathrm{Pa \cdot s}$	$0.15\,\mathrm{W/(m \cdot K)}$, $50\,\mathrm{W/(m \cdot K)}$	$875\,\mathrm{kg/m^3}$	$1\,\mathrm{m/s}$

Discretization
In this section the fluid properties will be calculated throughout the compressor. In order to be able to do this certain assumptions are made:

- The vapor is compressed and heats up
- The liquid is compressed and heats up by heat transfer from the vapor

- The isentropic efficiency is constant throughout the compressor
- The vapor and liquid have equal pressures

The assumption that the isentropic efficiency is constant throughout the compression makes it possible to calculate the total enthalpy throughout the compressor. This is done using the pressure distribution as explained in section 5.3.2. The resulting isentropic total enthalpy and total enthalpy is shown in equation 5.42 and equation 5.43 respectively. The resulting enthalpy is shown in figure 5.11.

$$h_{T,isen}(\phi) = f(p(\phi), s_{suc}, X_T) \tag{5.42}$$

$$h_T(\phi) = h_{T,suc} + \frac{h_{T,isen}(\phi) - h_{T,suc}}{\eta_{isen}} \tag{5.43}$$

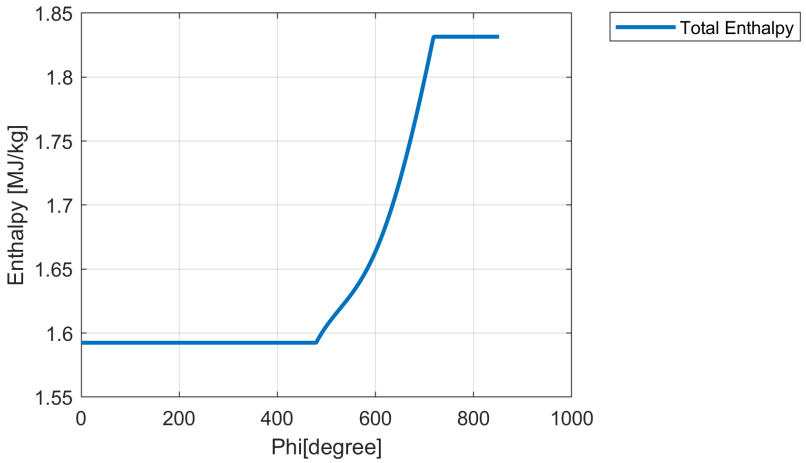

Figure 5.11: Total enthalpy throughout the compressor

The compressor is divided in smaller parts corresponding with a $\Delta\phi$. At the inlet the properties are calculated by adding the flows from the liquid and vapor line to the flow from the gap seal as discussed in section 5.3.2. These serve as the properties of the first control volume. Control volumes will be indicated with the superscript i. This gives the following set of initial properties:

$$h_L^{i=1} = h_{suc,L} \tag{5.44}$$
$$h_V^{i=1} = h_{suc,V} \tag{5.45}$$
$$\dot{m}_L^{i=1} = \dot{m}_{suc,L} \tag{5.46}$$
$$\dot{m}_V^{i=1} = \dot{m}_{suc,V} \tag{5.47}$$
$$X_L^{i=1} = X_{suc,L} \tag{5.48}$$
$$X_V^{i=1} = X_{suc,V} \tag{5.49}$$

At each control volume calculation the properties are first assumed to be equal to the previous control volume. The whole procedure is repeated in order to receive convergence. First the new vapor enthalpy is calculated using equation 5.50.

$$h_V^i = \frac{h_T^i \cdot \dot{m}_T - h_L^i \cdot \dot{m}_L^i}{\dot{m}_V^i} \tag{5.50}$$

This initially attributes the entire enthalpy increase to the enthalpy increase of the vapor. Consequently the vapor temperature is calculated using equation 5.51

$$T_V^i = f(p^i, h_V^i, X_V^i) \tag{5.51}$$

With this new vapor temperature the heat transfer between the liquid and vapor phase is calculated using equation 5.52. Here the heat transfer is calculated at each control volume in order to account for the change in fluid properties.

$$\dot{Q}^i_{VL} = h^i_{VL} \cdot dA^i \cdot (T^i_V - T^i_L) \tag{5.52}$$

The heat transfer to the oil is calculated using equation 5.53.

$$\dot{Q}^i_{LO} = U^i_{LO} \cdot (T^i_L - T^i_O) \tag{5.53}$$

This heat can potentially contribute to two things: the heating of the liquid and the evaporation of the liquid. In order to determine the magnitude of those effects the saturation temperature of the liquid is calculated using equation 5.54.

$$T^i_{sat,L} = f(p^i, q = 0, X^i_L) \tag{5.54}$$

If $T_{sat,L} > T_L$ (a part of) the heat goes into the heating of the liquid. First the amount of energy that is required in order to reach the saturation temperature is calculated using equation 5.55

$$\dot{Q}^i_{sat} = c^i_{p,L} \cdot (T^i_{sat,L} - T^i_L) \cdot \dot{m}^i_L \tag{5.55}$$

If $\dot{Q}^i_{sat} \geq \dot{Q}^i_{VL}$ the liquid temperature is calculated using equation 5.56. If $\dot{Q}^i_{sat} < \dot{Q}^i_{VL}$ the new liquid temperature becomes the saturation temperature and the amount of evaporation is calculated using equation 5.57.

$$T^i_L = T^{(i-1)}_L + \frac{\dot{Q}^i_{VL}}{\dot{m}^i_L \cdot c^i_{p,L}} - \frac{\dot{Q}^i_{LO}}{\dot{m}^i_L \cdot c^i_{p,L}} \tag{5.56}$$

$$\dot{m}^i_{evap} = \frac{\dot{Q}^i_{VL} - \dot{Q}^i_{sat}}{h^i_{evap}} \tag{5.57}$$

Here h^i_{evap} is the enthalpy of evaporation. At the end of each iteration the liquid and vapor massflows, compositions and enthalpies are calculated in order to preserve continuity. The massflows are calculated using equation 5.58, the enthalpies using equation 5.59 and the enthalpies using equation 5.60.

$$\begin{aligned} \dot{m}^i_L &= \dot{m}^{i-1}_L + \dot{m}^i_{evap} \\ \dot{m}^i_V &= \dot{m}^{i-1}_V - \dot{m}^i_{evap} \end{aligned} \tag{5.58}$$

$$\begin{aligned} \dot{X}^i_L &= (X^{i-1}_L \cdot \dot{m}^{i-1}_L - \dot{m}^i_{evap} \cdot X^i_{evap})/\dot{m}^i_L \\ \dot{X}^i_V &= (X^{i-1}_V \cdot \dot{m}^{i-1}_V + \dot{m}^i_{evap} \cdot X^i_{evap})/\dot{m}^i_V \end{aligned} \tag{5.59}$$

$$\begin{aligned} h^i_L &= f(T^i_L, p^i, X^i_L) \\ h^i_V &= \frac{h^i_T \cdot \dot{m}_T - h^i_L \cdot \dot{m}^i_L}{\dot{m}^i_V} \end{aligned} \tag{5.60}$$

At the end of each iteration the total enthalpy is lowered in order to account for the heat lost to the cooling oil during compression. This is calculated using equation 5.61.

$$h_T = h_T - \frac{\dot{Q}^i_{LO}}{\dot{m}_T} \tag{5.61}$$

Isentropic efficiency calculation

To keep track of the total amount of heat removed by the oil is important. This is because when neglecting this will result in a higher value of the isentropic efficiency since the discharge enthalpy is lowered. This is avoided by calculating the isentropic efficiency as if all the heat transfer with the oil happens when the fluid

already has been discharged. This discharge state will be called the adiabatic state and will be used to perform the isentropic efficiency calculations. The heat taken away by the oil cooler will be added to the absorber duty. The isentropic efficiency will be calculated using equation 5.62

$$\eta_{is} = \frac{h_{dis,isen} - h_{suc}}{h_{dis,ad} - h_{suc}} \tag{5.62}$$

Note that here the discharge enthalpy is in the nominator and $h_{dis,ad} > h_{dis}$. Not accounting for the the heat taken away by the oil cooler will result in a higher value for the isentropic efficiency. Equation 5.63 is used to calculate $h_{dis,ad}$.

$$h_{dis,ad} = h_{dis} + \frac{\dot{Q}_{LO}}{\dot{m}_{dis}} \tag{5.63}$$

5.4. Results

In this section the compressor performance will be analyzed. In this performance analysis special care will be given to compressors potential if the gap seal flow can be reduced. For this section the performance of 28 runs performed in 2020 will be reviewed. These runs all were performed under different operating parameters. In the performance analysis special attention will be given at performance as a function of pressure ratio and inlet vapor quality. Pressure ratio is a measure of how well the mixture was able to be compressed. The performance compared to the inlet vapor quality is interesting because the liquid is used to seal the compressor. On the other could to much liquid flow result in more friction.

Where available these results will be compared against the analysis of Infante Ferreira [30] and the model developed by Brancaccio [29]. The analysis of Infante Ferreira consists of the same raw data as this analysis, however it does consider the compressor discharge thermometers reading to be equal to the liquid temperature and it does calculate the process side heat loss to the oil by assuming that all the mechanical and driver losses are absorbed by the oil cooler and the remainder is lost to the process side. The analysis does consider the gap seal flow as well as a heterogeneous discharge flow. The model of Brancaccio is based on a compressor model that is based on the reference compressor scaled to match the experimental compressor geometry. This model does consider the gap seal flow as well as heterogeneous discharge flow, it however also assumes an adiabatic compression. The results from Infante Ferreira will be denoted with IF and the results from Brancaccio will be denoted with Br.

5.4.1. Heat transfer

In this section the heat transfer that occurs during the compression is reviewed. First the vapor to liquid heat transfer and the resulting temperature profiles in the compressor are analyzed. Second the liquid to oil heat transfer is quantified. Both of these heat transfers have an influence on the composition and properties of the flow at the compressor outlet and through the gap seal.

Vapor to liquid

The calculation of the vapor to liquid heat transfer is discussed in section 5.3.2. This calculations are applied on a set of data which parameters are given in table 5.3.

Table 5.3: Input properties into compressor model

p_{suc}	p_{dis}	T_{suc}	η_{is}	$\dot{m}_{L,suc}$	$\dot{m}_{V,suc}$	$X_{L,suc}$	$X_{V,suc}$
1.7 bar	4.7 bar	67 °C	0.7	22 kg/h	108 kg/h	0.17	0.86

These inputs were inserted into the compressor model and resulted in the temperature distribution as shown in figure 5.12

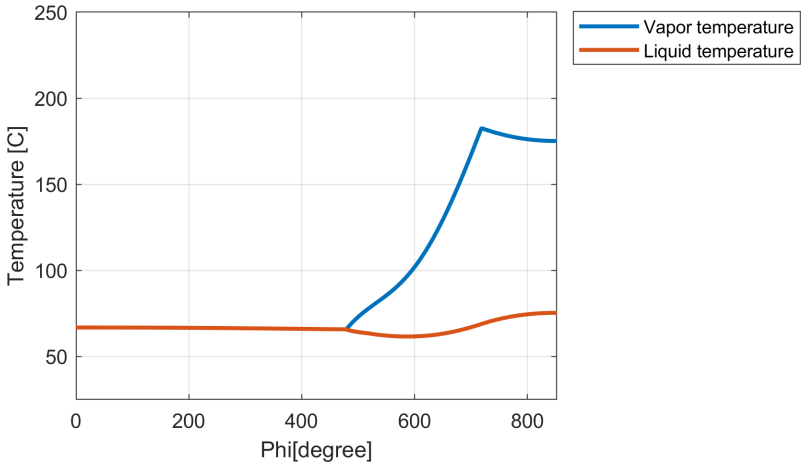

Figure 5.12: Temperature throughout the compressor

It can be seen that the temperature at the inlet of the compressor is more or less constant. This is due to the assumption that the vapor and liquid are at equilibrium at the compressor inlet. During the compression the vapor heats up and exchanges heat with the liquid. Because of the effect of the cooling oil the liquid temperature barely changes compared to the inlet temperature. This also means that evaporation is kept to a minimum as the liquid bulk temperature is below the saturation temperature for a large portion of the compression. In figure 5.13 the heat transfer coefficients for both vapor to liquid and liquid to oil are shown. Here it can be seen that the heat transfer coefficient increases when the vapor heats up at the compressor outlet.

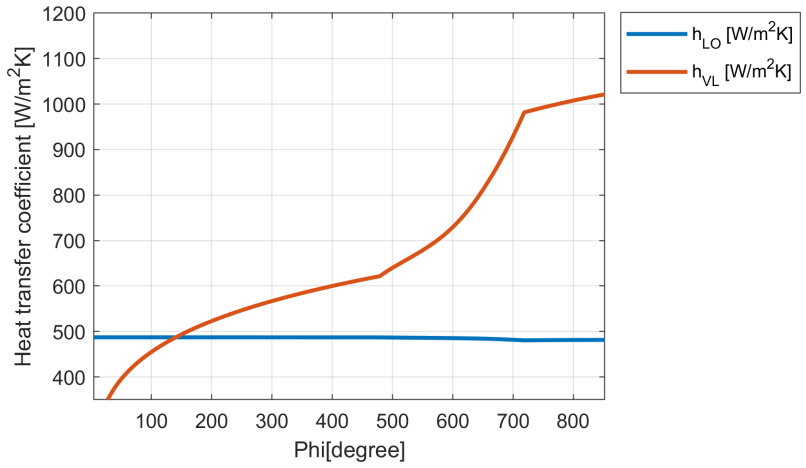

Figure 5.13: Vapor liquid heat transfer coefficient throughout the compressor

Liquid to oil

Understanding the heat loss to the lubrication oil is important as pointed out in section 5.3.2. The heat transfer coefficient is calculated at each segment of the compressor and is mostly influenced by the properties of the oil on the oil side. The heat transfer coefficient is shown in figure 5.13. The total amount of heat absorbed by the oil was calculated for all the data sets analyzed. In figure 5.14 and figure 5.15 the amount of heat is plotted against the pressure ratio and the vapor quality respectively.

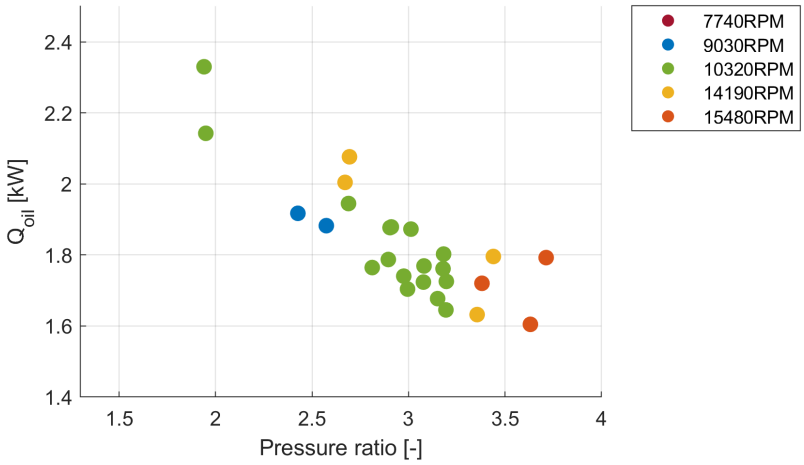

Figure 5.14: Heat taken up by oil as function of the pressure ratio

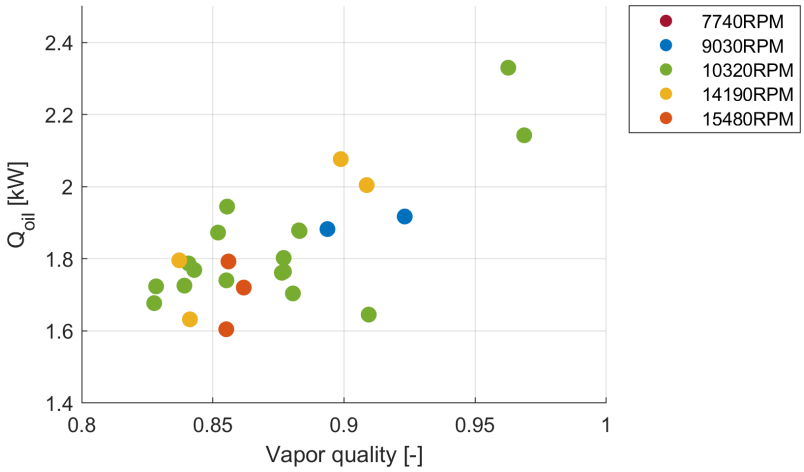

Figure 5.15: Heat taken up by the oil flow as function of the inlet vapor quality

Here it can be seen that the heat to the oil tends to be higher when the pressure ratio is lower. This can be explained when looking at figure 5.16. The cases where the pressure ratio is lower also tend to have a higher compressor suction temperature resulting in a larger temperature difference with the cooling oil.

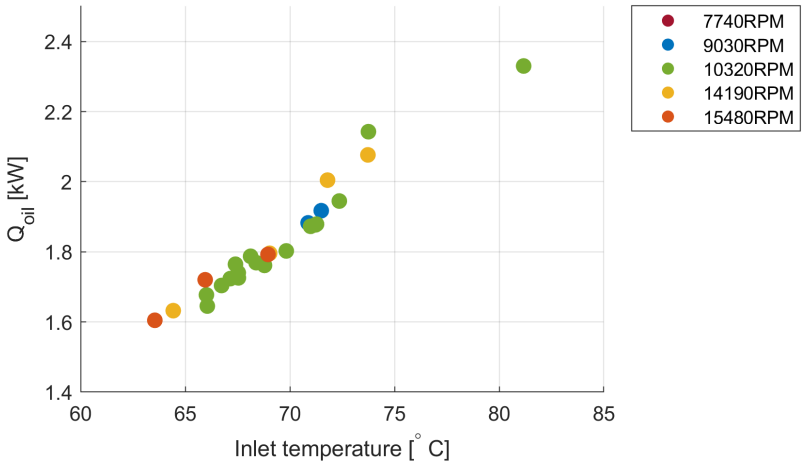

Figure 5.16: Heat taken up by oil as function of the inlet temperature

The total amount of heat taken up by the oil is mostly in the 1.5 kW to 2.0 kW range. The total oil cooler duty was between 3.0 kW and 4.5 kW. This means that there is a significant amount of the oil cooler duty that also cools the mechanical losses that occur in the compressor gearbox. The effect of the oil cooling on the total specific enthalpy throughout the compression can be seen in figure 5.17.

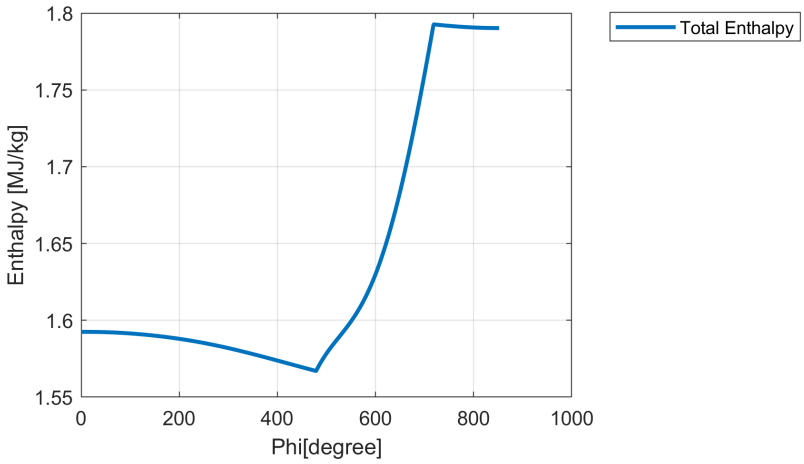

Figure 5.17: Total enthalpy throughout the compressor

5.4.2. Volumetric efficiency

The volumetric efficiency of a compressor is a measure of compressor performance. It compares the actual amount of fluid that is displaced by the compressor to the theoretical maximum displacement. In the case of the wet compressor used in this study the volumetric efficiency can be calculated as shown in equation 5.64.

$$\eta_{vol} = \frac{\dot{m}_{T,suc}}{\rho_{T,suc} \cdot V_{cav} \cdot N_m \cdot \omega} \tag{5.64}$$

Here V_{cav} is the maximum volume of a cavity, N_m is the male rotor lobes and ω is the rotational frequency. In figure 5.18 and figure 5.19 the volumetric efficiency is shown as a function of pressure ratio and inlet vapor quality respectively.

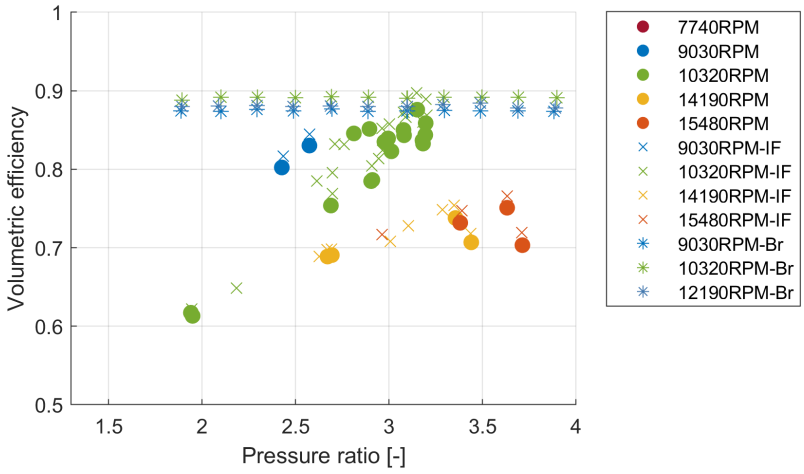

Figure 5.18: Volumetric efficiency as a function of pressure ratio

Figure 5.18 shows that the compressor seems to operate very well at its design pressure ratio of 3. It is also visible that the 9030 RPM and 10320 RPM outperform the other frequencies be some margin. The overall maximum value of around 0.88 indicates that there are little losses during the compression.

The results from Infante Ferreira do correlate well. The model from Brancaccio is almost insensitive to pressure ratio.

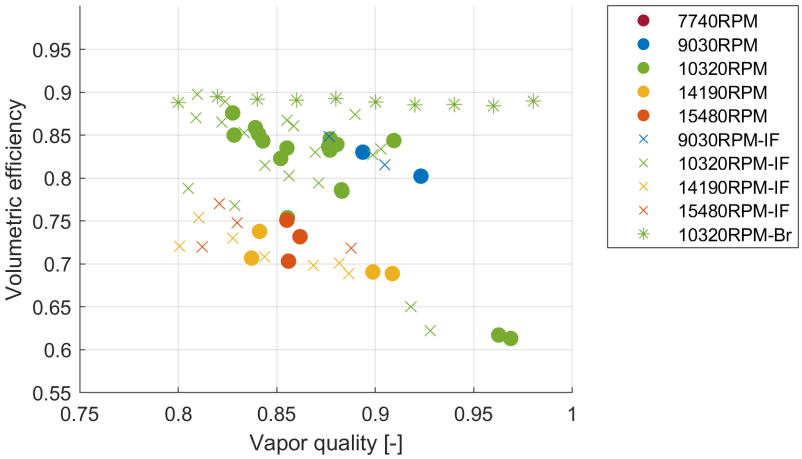

Figure 5.19: Volumetric efficiency as a function of inlet vapor quality

Figure 5.19 shows that the volumetric efficiency seems to be higher when the vapor quality is lower. This indicates that at lower vapor qualities the sealing by the liquid on the walls is effective and results in a better compression. This also explains why the outliers in figure 5.19 around the pressure ratio of 2 were lower, these cases have a very high inlet vapor quality and therefor it is expected that there is insufficient liquid in the compressor to provide an adequate seal. The results from Infante Ferreira do match up well but generally show a lower vapor quality. The model from Brancaccio is almost insensitive to the inlet vapor quality, this could indicate that the sealing effect from the liquid is not taken into account.

5.4.3. Isentropic efficiency

As discussed in section 4.3.2 and section 5.3.2 care has to be given when calculating the isentropic efficiency. To analyse the compressor performance four different approaches for the isentropic efficiency will be performed. In figure 5.20 the states around the compressor are shown once again.

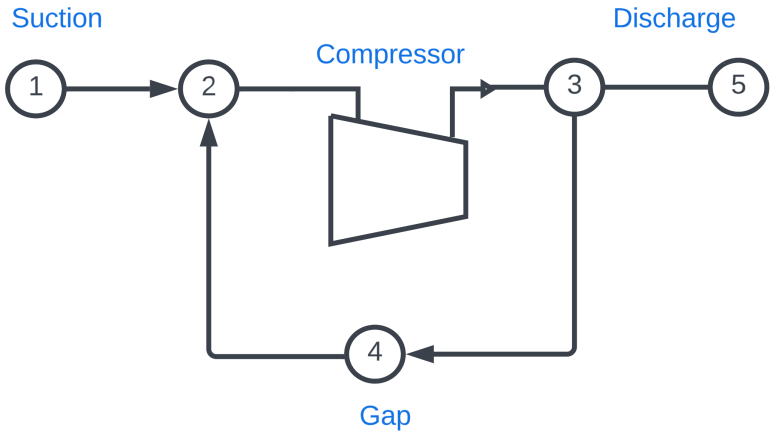

Figure 5.20: States around the compressor

There are two distinctions that have to be made. First is to calculate of the isentropic efficiency of the whole system including the gap seal flow or to calculate the isentropic efficiency of just the compressor. As concluded in section 4.3.2 the isentropic efficiency of just the compressor will always be higher compared to the total isentropic efficiency. When the total efficiency is concerned this will be marked with the subscript $_{tot}$.

The second distinction that has to be made is the distinction between adiabatic compression and non adiabatic compression. Assuming the compression to be adiabatic will result in higher efficiencies because the irreversibilities are masked by the heat taken away by the cooling oil. The non adiabatic case will be applied unless stated otherwise and will be calculated using equation 5.62 and equation 5.63. In figure 5.21 and figure 5.22 the compressor isentropic efficiencies are shown. These values are calculated using equation 5.65.

$$\eta_{is,comp} = \frac{h_{3,is} - h_2}{h_{3,ad} - h_2} \tag{5.65}$$

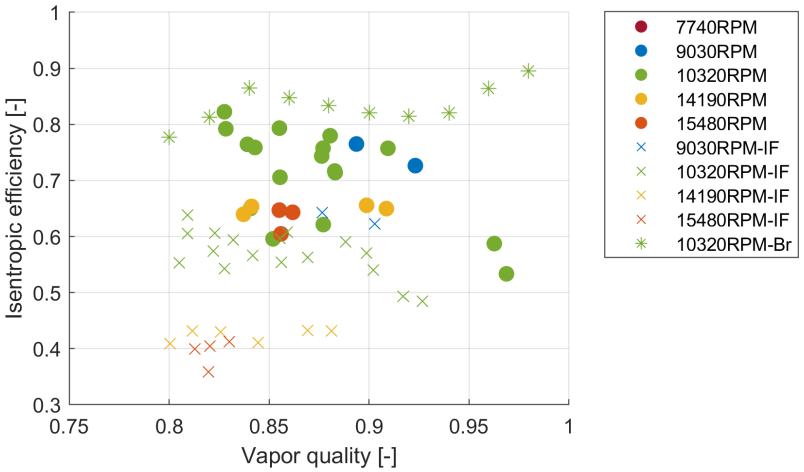

Figure 5.21: Isentropic efficiency as a function of inlet vapor quality

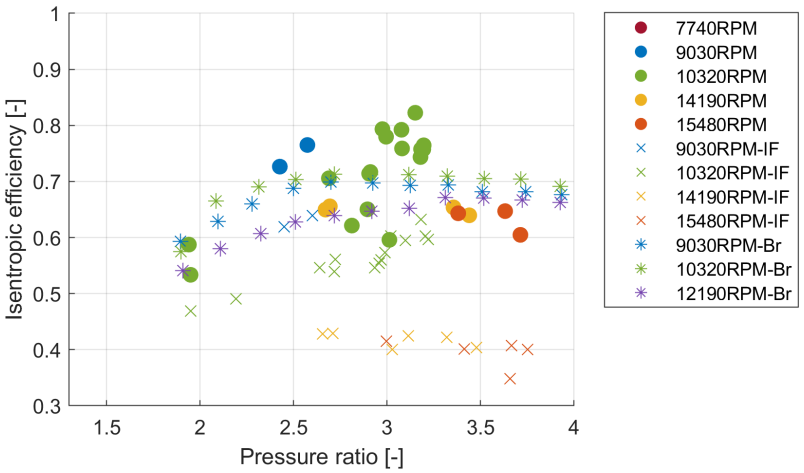

Figure 5.22: Isentropic efficiency as a function of pressure ratio

Both of these show the same trend as the volumetric efficiency. Lower vapor qualities and a pressure ratio around 3 seem to be preferred. The 9030 RPM and 10320 RPM cases seem to perform best. The analysis from Infante Ferreira generally shows a lower isentropic efficiency and a lower inlet vapor quality. The model from Brancaccio is generally in the same range, it has to be noted however that the increase in isentropic efficiency with higher inlet vapor qualities shows an opposite trend. When the compressor compresses almost only vapor it is very likely that the sealing and therefor compressor performance becomes worse.

The total isentropic efficiency is calculated using equation 5.66. The resulting total isentropic efficiency is plotted in figure 5.23. This is only plotted against the pressure ratio since the comparison against the vapor

quality at point 1 would not be entirely representative of the actual compressor condition. Consequently the total system isentropic efficiency is shown. The system isentropic efficiency is calculated using equation 5.67 and shown in figure 5.24

$$\eta_{is,tot} = \frac{h_{5,is} - h_1}{h_{5,ad} - h_1} \tag{5.66}$$

$$\eta_{is,sys} = \frac{\dot{m}_1 \cdot (h_{5,is} - h_1)}{\dot{W}_{elec}} \tag{5.67}$$

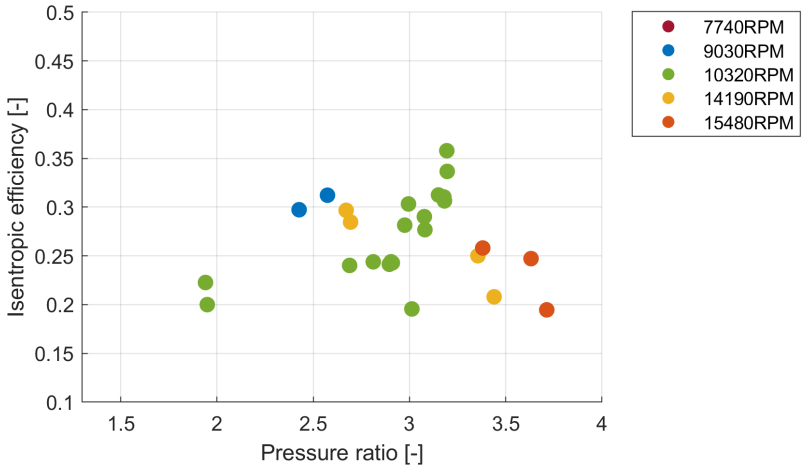

Figure 5.23: Total isentropic efficiency as a function of pressure ratio

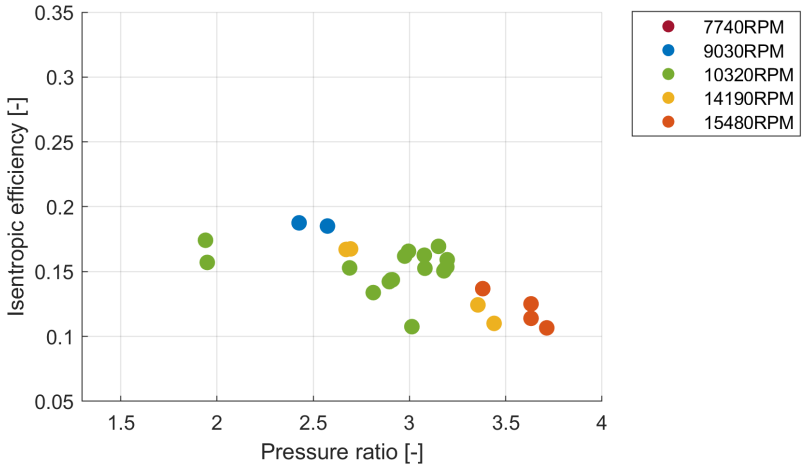

Figure 5.24: System isentropic efficiency as a function of pressure ratio

This result shows a large deviation from the results seen in figure 5.22. The difference between figure 5.23 and figure 5.24 also indicate that the mechanical losses in the system are large. The difference between the total isentropic efficiency and the compressor isentropic efficiency can be explained by the size of the gap seal flow. The gap seal flow factor compared to the pressure ratio is shown in figure 5.25. Here the gap seal flow is presented as a fraction of the total flow at point 1 $\dot{m}_1$.

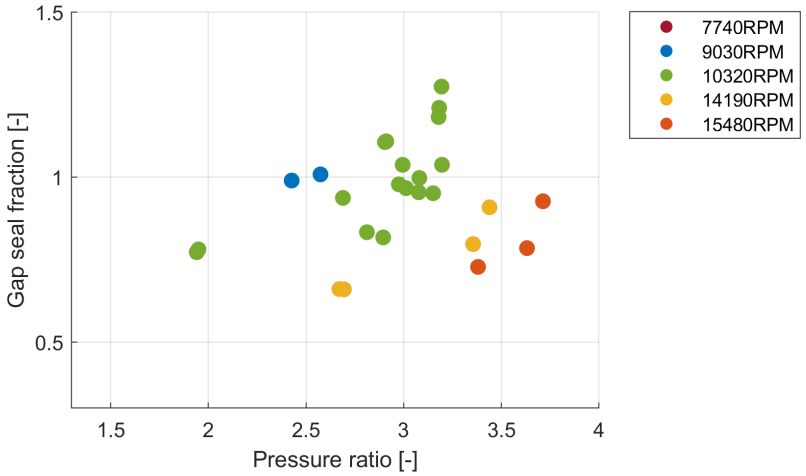

Figure 5.25: Gap seal fraction as function of pressure drop

This gap seal flow is high compared to the mass flow in the rest of the system. Decreasing the gap seal flow will be a way to increase the system performance while requiring less energy. When neglecting the gap seal flow it can result in underestimating the flow rate through the compressor as well as misinterpreting the mixture composition.

Finally the impact of the adiabatic calculation scheme is shown. In figure 5.26 the results between the adiabatic calculation and non adiabatic calculation scheme are compared. It is clear that not taking into account the oil heat loss during compression leads to results that are unrealistically high.

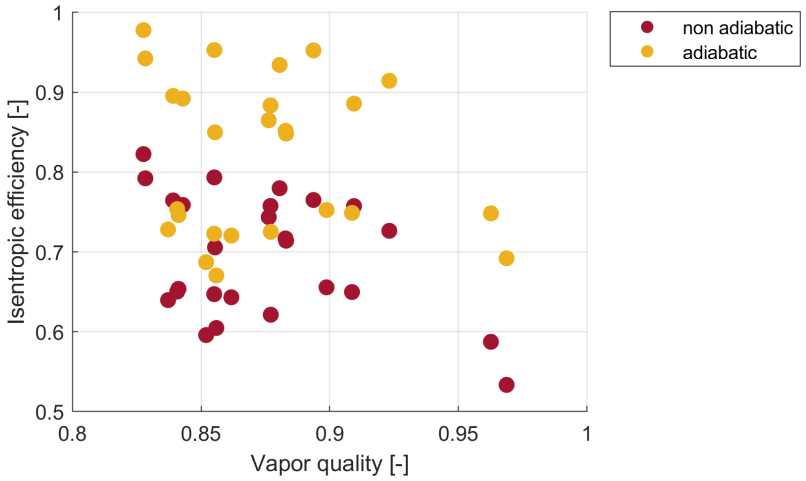

Figure 5.26: Adiabatic and non adiabatic calculation scheme compared

5.4.4. Pressure drop

The pressure drop was computed for all the data sets. Generally the pressure drop was between 0.05 bar and 0.3 bar. As can be seen in figure 5.27 the pressure drop is mainly depended on the total mass flow rate. There is one outlier which shows a high pressure drop even when the total flow rate was relatively low. This can be explained when viewing figure 5.28. Here it is visible that the outlier has an exceptional high vapor content at the compressor inlet which results in high vapor content at the outlet. The high discharge vapor content results in higher flow velocities and therefor higher pressure drops.

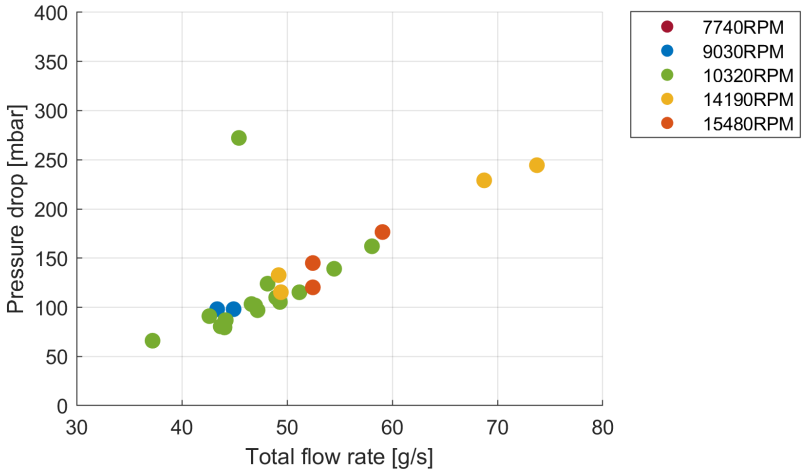

Figure 5.27: Pressure drop as a function of total mass flow rate

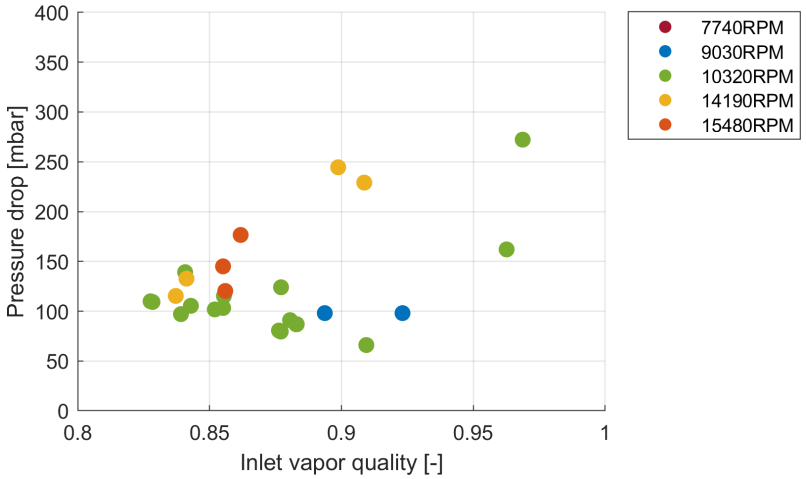

Figure 5.28: Pressure drop as a function of inlet vapor quality

The impact of the pressure drop on the liquid and vapor composition is illustrated in figure 5.29 and figure 5.30. It can be seen that for both the liquid and the vapor the ammonia content is slightly lower when considering the pressure drop. This in turn will have an effect of estimating a lower the ammonia concentration at the inlet of the compressor.

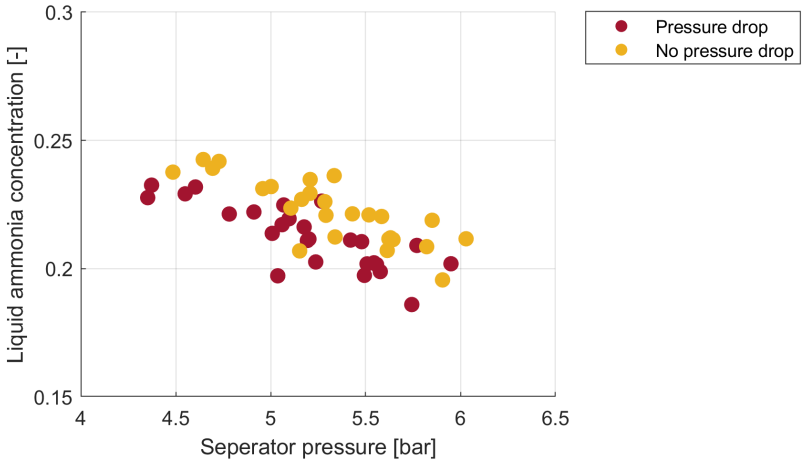

Figure 5.29: Liquid ammonia concentration as function of separator pressure

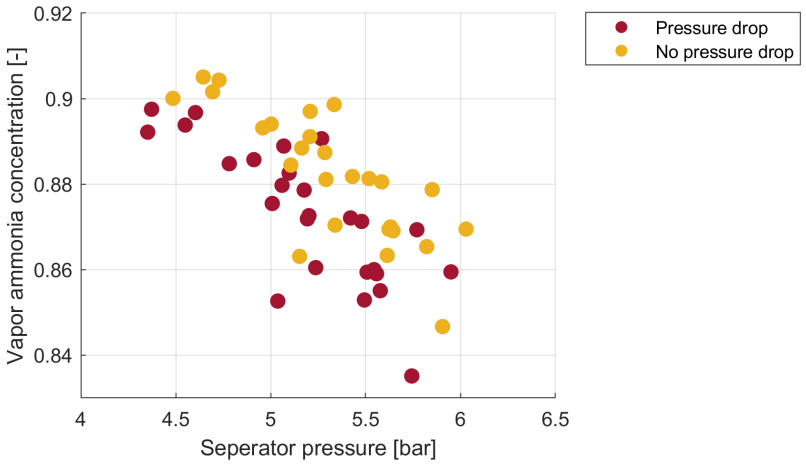

Figure 5.30: Vapor ammonia concentration as function of separator pressure

6

Economical and energetic comparison of heat pump technology

The heat pump is a technology that is already widespread in the industry. CRHP's aim to improve over existing VCHP's in operating range and efficiency. HACHP's utilizing dry compression have already showed promising performance compared to existing technology at the cost of more complexity. CRHP's utilizing wet compression promise to be able to operate at higher temperatures compared to both VCHP's and HACHP's. Once more mature the wet compression should not add too much complexity and therefor cost to a high temperature heat pump (HTHP). In order to properly access the performance of the CRHP a case study is performed where the performance of CRHP's and VCHP's is compared against an electrical boiler on an energetic and economic basis. These technologies will be compared over one realistic industrial application where HTHP's do have potential over conventional technologies.

6.1. Waste heat recovering using heat pumps

All the heat pumps technologies described above are able recover waste heat. In this section the way this can be done is shown. In figure 6.1 a T-h diagram is plotted for a compression resorption cycle. The waste heat temperature is below the absorber outlet temperature and above the desorber inlet temperature. This means that at the cold side the waste heat can be used to heat up the mixture and evaporate almost all the working fluid. At the hot side the stream of not usable temperature can be upgraded to useful levels. This results in one stream at close to ambient temperature and one stream at elevated, usable temperature.

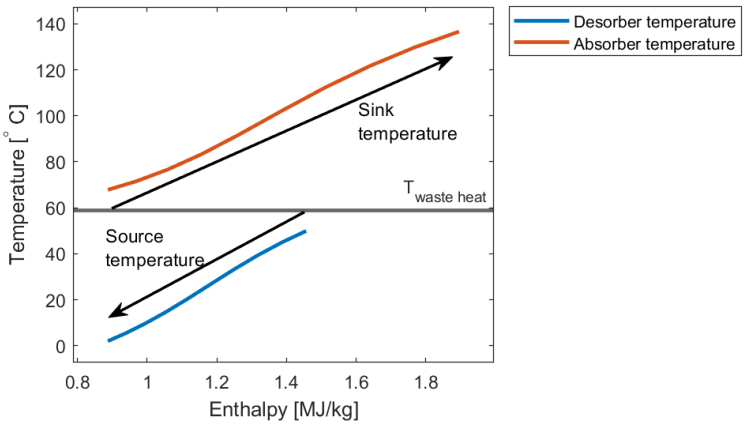

Figure 6.1: T-h diagram for utilizing waste heat

6.2. Paper recycling

This case study will look at a case with large potential for the application of HTHP's. Heat pumps are especially suitable for applications where there is both a heating and a cooling requirement. This case

focuses on upgrading waste heat in the paper sector. The paper sector has one of the highest low grade heating demands across all industries [8]. While also releasing waste heat at the around 60°C [46].

Paper recycling is an important and energy demanding process. Making use of recycled pulp gives an energy reduction of around 40% compared to the use of unrecycled pulp [47]. On top of that recycling paper also reduces the amount of wood that needs to be harvested. In order to conclude where best to apply heat pumps it is important to first understand the paper recycling process. This is illustrated in figure 6.2

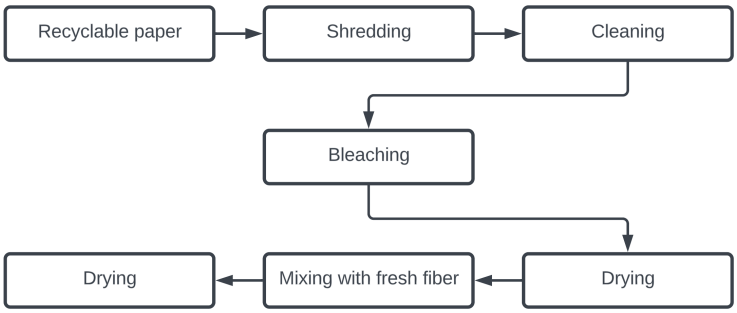

Figure 6.2: Paper recycling process

The most important processes that involve heat are the bleaching process and the drying process. The relevant thermodynamic properties of interest are shown in table 6.1.

Process	Temperature range	Waste heat temperature	Fraction of heating demand
Bleaching	80 °C - 150 °C	60 °C	20% - 30%
Drying	120 °C - 200 °C	100 °C	50 % - 70%

Table 6.1: Typical temperature ranges and heating demand distribution of paper recycling [46] [48]

Here the 60°C waste heat would normally be mostly rejected to the environment and not be used for something useful. For this case the waste heat of both processes will be utilized by the use of different kind of heat pump technologies. For this case cycles will be designed to upgrade waste heat from $60\,°$C to up to $135\,°$C.. It will be investigated how suitable the technologies are for producing 1 MW of upgraded waste heat.

6.2.1. Energetic

In this section the energetic performance of the different heat pump technologies will be compared. The global assumptions for all the heat pump technologies are:

- The total mechanical and electric efficiency is taken as 90% for all heat pump technologies
- Pressure drops over the heat exchangers is neglected
- Dry compression isentropic efficiency is estimated at 80%
- Expansions are isenthalpic

For the economic and energetic performance the influence of differing minimal thermal driving force in the heat exchangers is varied between 3 K and 10 K. A small driving force means higher energetic efficiency but a higher equipment cost as well. For the wet compression the isentropic efficiency is varied between 60% and 80 % this will give an indication at which point the CRHP will be energetically and economically competitive against existing technology.

VCHP

The VCHP modelled is shown in figure 6.3. First a working fluid has to be selected. This VCHP utilises a pure fluid which needs to be selected specifically for this application. The selection of a working fluid is

described in Appendix B.1. The chosen working fluid is butane. Butane has a reasonable GWP and is able to operate at the lowest pressure ratio, reducing cost.

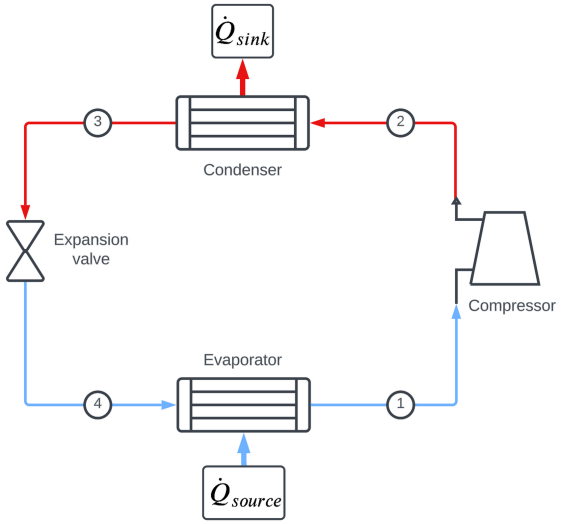

Figure 6.3: Layout VCHP

The governing equations used to model the VCHP are described in Appendix B.2. The performance of the heat pump is very depended on the temperature at which the evaporation takes place, as can be seen in figure 6.4. Here T_{cold} is the exit temperature of the waste heat stream in the condenser. Here it is necessary to have a reasonable temperature difference to the waste heat temperature to serve as the heat source. This can be explained when looking at equation 6.1. When there is a small temperature difference between the waste heat and the evaporator temperature the mass flow of the cooling water through the evaporator has to become higher. The amount of upgraded waste heat released by the heat sink is directly related to the heat absorbed in the heat source as can be seen in equation 6.2. Therefore the cold temperature of $25\,^{\circ}$C should be used.

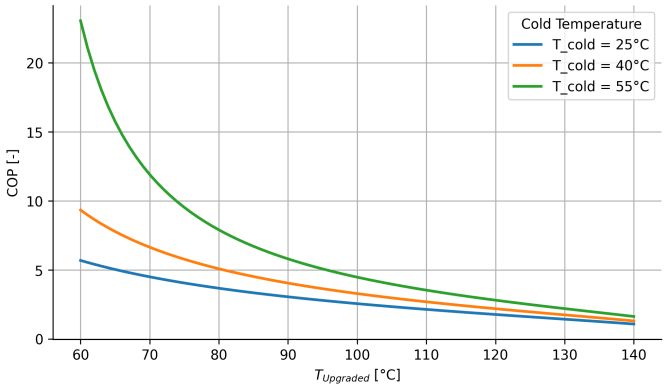

Figure 6.4: COP as a function of upgraded waste heat temperature

$$\dot{Q}_{source} = \dot{m}_{cw} \cdot c_{p,cw} \cdot (T_{wh} - T_{cold}) \tag{6.1}$$

$$\dot{Q}_{sink} = \dot{W}_{comp} + \dot{Q}_{source} \tag{6.2}$$

Based on figure 6.4 the upgraded waste heat temperature is chosen at $110\,°C$. This should still yield a reasonable COP while also upgrading the waste heat to a level where it is usable for bleaching. In table 6.2 the energy required to produce $1\,MW$ of is shown. This is evaluated for different thermal driving forces.

Table 6.2: VCHP performance at different thermal driving forces in the heat exchangers

T_{dr}	$5\,K$	$10\,K$
COP	2.01	1.72
$\dot{W}_{elek}$	$0.54\,MW$	$0.64\,MW$
$\dot{Q}_{sink}$	$1\,MW$	$1\,MW$
$\dot{Q}_{source}$	$0.50\,MW$	$0.42\,MW$
T_{cold}	$25\,°C$	$25\,°C$
T_{hot}	$110\,°C$	$110\,°C$
PR	$9.74\,bar$	$12.6\,bar$

CRHP

The CRHP offers great promise for upgrading waste heat. A schematic drawing of the CRHP considered in this study is shown in figure 6.5 The governing equations used for modelling the CRHP used in this study are displayed in Appendix B.3.

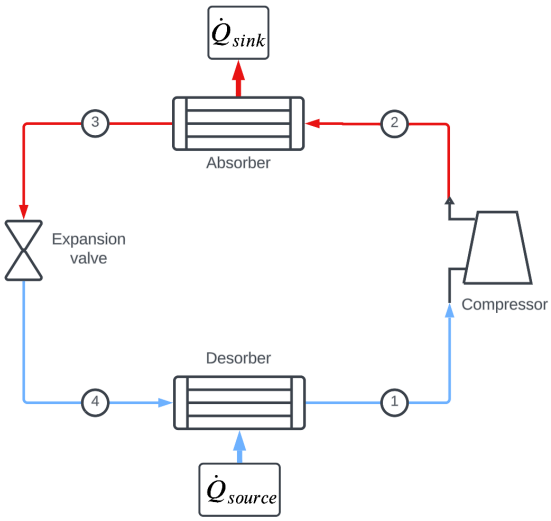

Figure 6.5: Layout CRHP

The performance of this CRHP is strongly connected to the ammonia concentration of the mixture. In figure 6.6 the impact of the ammonia concentration on the COP is shown. It can be seen that for low ammonia concentrations the COP is high. It has to be taken into account however that at lower temperature lifts the COP is generally higher. This can be seen in figure 6.7, when upgrading waste heat to $150\,°C$ the COP drops to around 3.

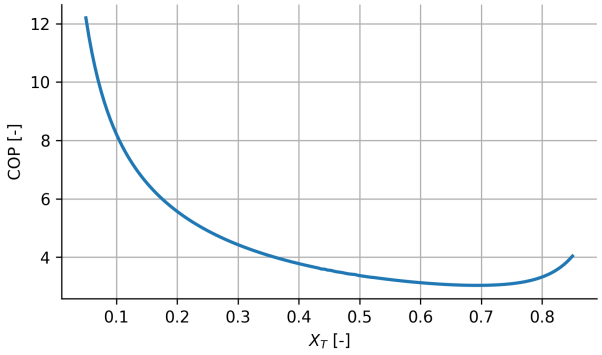

Figure 6.6: COP as function of total ammonia concentration

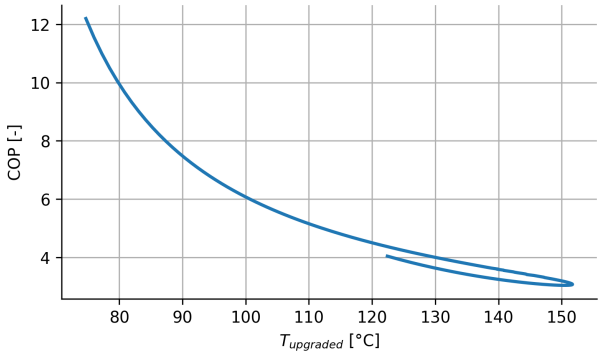

Figure 6.7: COP as a function of upgraded waste heat temperature

For this analysis the performance of the CRHP when upgrading waste heat to $135\,°$C will be evaluated. It can be seen in figure 6.7 that at $135\,°$C there is still a reasonable COP of around 3.7. The figure shows that at there are two possible ammonia concentrations which will be able to achieve an upgraded waste heat temperature of $135\,°$C. Both of these concentration are reviewed for different thermal driving forces in table 6.3. This analysis is performed for an isentropic efficiency ranging from 60% to 80%. While the cases with the low ammonia concentration have a higher COP, it has to be noted that the pressure ratio between the hot and cold side is a lot higher compared to the case with the higher ammonia concentration. This is clearly visible in figure 6.8.

Table 6.3: CRHP performance at different thermal driving forces for an isentropic efficiency ranging from 60% to 80%

T_{dr}	$5\,$K	$10\,$K	$5\,$K	$10\,$K
COP	3.36-3.96	3.31-3.56	3.05-3.46	2.75-3.09
$\dot{W}_{elek}$	0.33-$0.28\,$MW	$0.33-0.31\,$MW	$0.36-0.32\,$MW	$0.40-0.36\,$MW
$\dot{Q}_{sink}$	$1\,$MW	$1\,$MW	$1\,$MW	$1\,$MW
$\dot{Q}_{source}$	$0.70-0.75\,$MW	$0.70-0.72\,$MW	$0.67-0.71\,$MW	$0.64-0.68\,$MW
T_{cold}	$14.1-11.0\,°$C	$23.4-13.9\,°$C	$4.1--1.1\,°$C	$6.5-0.2\,°$C
T_{hot}	$135\,°$C	$135\,°$C	$135\,°$C	$135\,°$C
PR	18.1-19.9	20.8-29.1	7.90-10.4	9.98-13.9
X_T	0.37-0.41	0.30-0.40	0.82-0.80	0.83-0.80

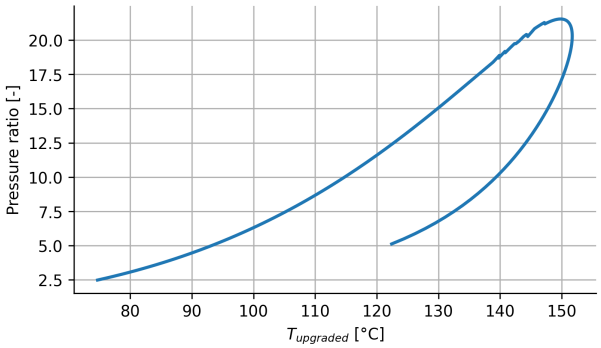

Figure 6.8: Pressure ratio as a function of waste heat temperature

From an energetic perspective the case with a low thermal driving force of $5\,\mathrm{K}$ and low ammonia concentration of $X_T = 0.40$ it the best. The drawback of the lean ammonia solution however is that the pressure drop is larger. The difference between a low and high isentropic efficiency results in a noticeable effect on the energetic performance of the CRHP. When using a small thermal driving force with the rich ammonia solution the cold temperature could be less than the freezing point of water. This is not desirable and if an isentropic efficiency of 0.8 would be achieved this needs to be accounted for.

Electric boiler
An electric boiler can also be used to upgrade a waste heat stream to usable levels. For this study the efficiency of an electrical boiler is taken as 100%. This means that for every kW of electricity one kW of heat is added to the waste heat stream. This is low compared to the 1.5 to 4 case of the heat pumps. An electrical boiler is simpler compared to the heat pumps which may significantly shorten it's payback time. One benefit of the electric boiler compared to a gas boiler is that it is also able to run on renewable energy. Theoretically a gas boiler can run on renewable fuels as well but this might be more costly and greenhouse gasses would still be emitted.

6.2.2. Economic

All cases will be compared against a gas boiler which is already in place in the paper plant. In order to calculate the yearly savings and payback time the cost of electricity and gas is necessary. For this the data from the CBS was used [49]. This means that the electricity price is assumed at 260€ per MWh and gas price at 159€ per MWh. When carbon tax prices of 70€ per ton are considered the gas price becomes 173€ per MWh [50].

Investment cost
To calculate the investment cost equation 6.3 is used [51]. Here a, b and n are constants based on the equipment specified and S relates to the size of equipment used, this is the area in m^2 for heat exchangers and power in kW for the compressor. This relation gives an indication for the installed system cost. The parameters were determined in 2012, to correct for this a correction factor $c_{inflation}$ is used. For this the producer price index is used [52] which results in $c_{inflation} = 1.31$.

$$C_{equipment,2012} = a + b \cdot S^n \tag{6.3}$$

$$C_{equipment,2024} = c_{inflation} \cdot C_{equipment,2012} \tag{6.4}$$

For the size of the heat exchangers equation 6.5 is used. The typical values for heat transfer coefficients are taken as $1000\,\mathrm{W/(m^2K)}$ for both the desorber and absorber of the CRHP. For the VCHP $1200\,\mathrm{W/(m^2K)}$ is used for the evaporator and $1500\,\mathrm{W/(m^2K)}$ is used for the condenser.

$$A = \frac{Q_{hx}}{U \cdot \Delta T_{ln}} \tag{6.5}$$

Where ΔT_{ln} is calculated using equation 6.6

$$\Delta T_{ln} = \frac{\Delta T_{hx,in} - \Delta T_{hx,out}}{ln(\frac{\Delta T_{hx,in}}{\Delta T_{hx,out}})} \tag{6.6}$$

VCHP
In table 6.4 the relevant properties to access the economic performance of a VCHP are shown. The complete table with all the duties and area's is shown in Appendix B.4. It can be seen that the version with the lower thermal driving force and therefor higher heat exchangers performs better and even results in a lower total investment cost. The payback time of 6 years is still large but could be economically viable.

Table 6.4: Economic performance of VCHP

T_{dr}	5 K	10 K
COP	2.01	1.72
Cost heat exchanger source	77 k€	35 k€
Cost heat exchanger sink	120 k€	63 k€
Cost compressor	1343 k€	1518 k€
Investment cost	1540 k€	1616 k€
Yearly savings	256 k€	44 k€
Payback time	6.0 years	36.7 years

CRHP
In table 6.5 the relevant properties to evaluate the economic performance of the different CRHP configurations is shown. The complete table with all the duties and area's specified is shown in Appendix B.5. All these results are given for an isentropic efficiency from 60% to 80%. The compressor cost was multiplied by a factor of two to compensate for the use of an oil free compressor [24].

Table 6.5: Economic performance of CRHP at different thermal driving forces and ammonia concentrations for isentropic efficiency ranging from 60% to 80%

T_{dr}	5 K	5 K	10 K	10 K
COP	3.36-3.96	3.31-3.56	3.05-3.46	2.75-3.09
X_T	0.37-0.41	0.82-0.80	0.30-0.40	0.83-0.80
Cost heat exchanger source	$126 - 133$ k€	$120 - 127$ k€	$65 - 67$ k€	$60 - 63$ k€
Cost heat exchanger sink	175 k€	175 k€	91 k€	91 k€
Cost compressor	$2080 - 1830$ k€	$1934 - 1750$ k€	$2106 - 1990$ k€	$2098 - 1934$ k€
Investment cost	$2378 - 2138$ k€	$2229 - 2052$ k€	$2262 - 2148$ k€	$2249 - 2088$ k€
Yearly savings	$762 - 876$ k€	$751 - 805$ k€	$686 - 784$ k€	$595 - 696$ k€
Payback time	3.1-2.4 years	3.0-2.6 years	3.2-2.7 years	3.8-3.0 years

All of these show short payback times and high yearly savings. The more expensive heat exchanger tend to outperform the cheaper ones since the compressor is the largest contributor to the total heat pump cost. While the isentropic efficiency does have a noticeable impact on the economic performance the results tend to be between a year in payback time and both the 60% and 80% isentropic efficiency seems to be economically viable.

Electric boiler
An electric boiler with a capacity of 1 MW costs around 180 k€ [53]. With the current energy prices considered the electrical boiler will be a more expansive solution compared to a gas boiler. It has to be noted that this may very well change with future price fluctuations especially for the carbon permits. The installation costs of an electric boiler is also low compared to the yearly energy cost which means that this solution can become more interesting in the future since it is a cheaper investment compared to the heat pumps.

6.2.3. Conclusion

In this chapter the performance of a VCHP,CRHP and an electric boiler for the use in a paper recycling plant were energetically and economically evaluated for the use in a paper recycling plant. Of these choices the CRHP shows the most promising results. The performance of the CRHP shows that for the chosen parameters the mixture that is leaner in ammonia performs better than the mixture that is rich in ammonia. The difference however is not large and it should be investigated further to have a more decisive conclusion. It could very well be that the higher pressures that are required in the case of the lean solution drive up the cost of the equipment more than anticipated resulting in a worse economic performance.

The VCHP seems to perform worse compared to the CRHP, the ability of the CRHP to match the temperature glides of the heat source and sink with the waste stream results in a lower average temperature lift and consequently a higher COP. It can be seen that when the COP gets to low that the yearly savings become to low to be economically viable.

7

Conclusion

7.1. Conclusion

The objective of this research was:

To find the operational conditions to maximize the performance of a high temperature compression resorption heat pump using wet compression by developing a cycle energy balance model.

A cycle model has been developed to analyse data from the experimental setup. Four limitations of the experimental setup were identified, The heterogeneous behavior, the gap seal flow, the cooling effect of the oil in the compressor housing and the pressure drop of the high pressure side. The following conclusions regarding the limitations are drawn:

- Taking into account the heterogeneous behavior is necessary to accurately analyse a twin screw wet compressor. The compression happens in a very small part of the compressor at a place where the liquid and vapor are likely not evenly distributed due to the centrifugal forces of the rotating rotors, reducing the heat transfer area. The heterogeneous behavior influences the measurements at the compressor exit as well as the properties of the gap seal flow. The gap seal flow properties are important in order to know the precise ammonia content and vapor quality inside the compressor. A difference of liquid and vapor temperature of around to 100 K was calculated at the compressor discharge.
- The influence of the gap seal flow on the compressor performance is large. The presence of the gap seal flow results in often more than double the flow through the compressor. When correcting for the gap seal flow the maximum isentropic efficiency of the compressor itself was up to 0.83, while the isentropic efficiency of the compressor ignoring the gap seal flow was only up to 0.36.
- The cooling oil in the compressor housing has a noticeable effect on the performance. Quantifying this heat loss is important to accurately determine the isentropic efficiency. Neglecting the effect of the oil cooling result in higher, unrealistic values for the isentropic efficiency.
- The pressure drop of the high pressure side of the system is between 0.05 bar and 0.3 bar. This pressure drop is important because the separator pressure is used to calculate the ammonia content in the liquid and vapor lines. Neglecting the pressure drop will result in an overestimation of the ammonia content.

Regarding the operating conditions of the wet compressor the following conclusions are drawn:

- The inlet vapor quality has a large effect on the isentropic efficiency of the compressor. When the inlet quality gets above 0.9 there is a noticeable drop in isentropic efficiency. This trend is also visible for the volumetric efficiency indicating that at higher vapor qualities the sealing effect of the liquid decreases.
- The gap seal flow has a large impact on the total isentropic efficiency of the compressor. The gap seal flow results in often double the flow through the compressor and with that it can more than half the effective isentropic efficiency of the compressor. The decreasing of the gap seal flow is directly related to a better total isentropic efficiency of the compressor.

- By considering the heat transfer between the liquid and vapor and between the liquid and oil it can be seen that the oil cooling results in a discharge liquid temperature that is not that different from the suction liquid temperature. This results in less evaporation inside the compressor which enables the liquid to act as lubricant.
- The experimental compressor has the highest isentropic efficiency at a rotational speed of 10320 RPM. At a slightly lower rotational speed or 9030 RPM the isentropic efficiency is still high. Operating at this lower rotational speed allows for operation at a lower pressure ratio.

A case study was performed where the application of a CRHP was compared against a VCHP and an electric boiler. The CRHP had the highest investment cost. However, with the highest COP of up to 3.96 when upgrading waste heat for 60 K to 135 K and a payback period as short as 2.4 years it was the best choice. The impact of the isentropic efficiency that the wet compressor is able to be achieved did impact the energetic performance, however the payback time was increased by only 0.7 years when the isentropic efficiency of the compressor was lowered form 80% to 60%. The VCHP seems to be just economically viable with a payback time of 6.0 years and a COP of up to 2.01. The electric boiler is with current pricing more expensive than a gas boiler and does not seem like a suitable alternative economically. Environmentally it might still be a choice due to its low price and ability to make use of sustainably produced electricity.

7.2. Recommendations

- A CFD study simulation the heat and mass transfer during compression should be performed for a better understanding of the compressor outlet properties.
- The best compressor performance was found at the lowest inlet vapor qualities of around 0.8, future tests should focus on a wider range of inlet vapor qualities.
- Placement of a temperature sensor at the absorber inlet will reduce the reliance on measurements in the heterogeneous parts of the setup.
- Placement of a pressure sensor at the separator will allow for more precise calculation of the liquid and vapor line compositions.
- Measurement of the gap seal flow will allow for a better calculation of the compressor isentropic efficiency.
- The reduction of the gap seal flow needs to be investigated. This will increase the overall compressor isentropic efficiency.
- The heat taken away from the process side needs to be measured in order to accurately correct for the non-adiabatic compression.
- The heterogeneous compression leads to high vapor temperatures at the compressor discharge. The effect of the high temperature on the reliability of seals and other components should be investigated.

References

[1] UNFCCC. *The Paris Agreement*. URL: https://unfccc.int/process-and-meetings/the-paris-agreement. (accessed: 01-10-2023).

[2] Hannah Ritchie, Max Roser, and Pablo Rosado. “Energy”. In: *Our World in Data* (2022). https://ourworldindata.org/energy.

[3] Eurostat. *Final energy consumption in industry - detailed statistics*. URL: https://ec.europa.eu/eurostat/statistics-explained/index.php?title=Final_energy_consumption_in_industry_-_detailed_statistics#The_largest_industrial_energy_consumers_in_the_EU. (accessed: 01-10-2023).

[4] Robert de Boer, Andrew Marina, Benjamin Zühlsdorf, Cordin Arpagaus, Michael Bantle, Veronika Wilk, Brian Elmegaard, José Corberán, and Jessica Benson. *Strengthening Industrial Heat Pump Innovation: Decarbonizing Industrial Heat*. 2020.

[5] Khalid Hamid, Uzair Sajjad, Marcel Ulrich Ahrens, Shuai Ren, P. Ganesan, Ignat Tolstorebrov, Adeel Arshad, Zafar Said, Armin Hafner, Chi-Chuan Wang, Ruzhu Wang, and Trygve M. Eikevik. “Potential evaluation of integrated high temperature heat pumps: A review of recent advances”. In: *Applied Thermal Engineering* 230 (2023), p. 120720. DOI: https://doi.org/10.1016/j.applthermaleng.2023.120720. URL: https://www.sciencedirect.com/science/article/pii/S1359431123007494.

[6] F. Schlosser, M. Jesper, J. Vogelsang, T.G. Walmsley, C. Arpagaus, and J. Hesselbach. “Large-scale heat pumps: Applications, performance, economic feasibility and industrial integration”. In: *Renewable and Sustainable Energy Reviews* 133 (2020), p. 110219. DOI: https://doi.org/10.1016/j.rser.2020.110219. URL: https://www.sciencedirect.com/science/article/pii/S1364032120305086.

[7] V. Gudjonsdottir and C.A. Infante Ferreira. “Technical and economic analysis of wet compression–resorption heat pumps”. In: *International Journal of Refrigeration* 117 (2020), pp. 140–149. DOI: https://doi.org/10.1016/j.ijrefrig.2020.05.010. URL: https://www.sciencedirect.com/science/article/pii/S0140700720302103.

[8] Cordin Arpagaus, Frédéric Bless, Michael Uhlmann, Jürg Schiffmann, and Stefan S. Bertsch. “High temperature heat pumps: Market overview, state of the art, research status, refrigerants, and application potentials”. In: *Energy* 152 (2018), pp. 985–1010. DOI: https://doi.org/10.1016/j.energy.2018.03.166. URL: https://www.sciencedirect.com/science/article/pii/S0360544218305759.

[9] Jonas K. Jensen, Torben Ommen, Wiebke B. Markussen, Lars Reinholdt, and Brian Elmegaard. “Technical and economic working domains of industrial heat pumps: Part 2 – Ammonia-water hybrid absorption-compression heat pumps”. In: *International Journal of Refrigeration* 55 (2015), pp. 183–200. DOI: https://doi.org/10.1016/j.ijrefrig.2015.02.011. URL: https://www.sciencedirect.com/science/article/pii/S0140700715000432.

[10] Anton A. Kiss, Servando J. Flores Landaeta, and Carlos A. Infante Ferreira. “Towards energy efficient distillation technologies – Making the right choice”. In: *Energy* 47.1 (2012). Asia-Pacific Forum on Renewable Energy 2011, pp. 531–542. DOI: https://doi.org/10.1016/j.energy.2012.09.038. URL: https://www.sciencedirect.com/science/article/pii/S0360544212007165.

[11] Opeyemi Bamigbetan, Trygve M. Eikevik, Petter Nekså, and Michael Bantle. “Review of vapour compression heat pumps for high temperature heating using natural working fluids”. In: *International Journal of Refrigeration* 80 (2017), pp. 197–211. DOI: https://doi.org/10.1016/j.ijrefrig.2017.04.021. URL: https://www.sciencedirect.com/science/article/pii/S0140700717301780.

[12] Petter Nekså, Håvard Rekstad, G.Reza Zakeri, and Per Arne Schiefloe. “CO2-heat pump water heater: characteristics, system design and experimental results”. In: *International Journal of Refrigeration* 21.3 (1998), pp. 172–179. DOI: https://doi.org/10.1016/S0140-7007(98)00017-6. URL: https://www.sciencedirect.com/science/article/pii/S0140700798000176.

[13] F. Ziegler and P. Riesch. “Absorption cycles. A review with regard to energetic efficiency”. In: *Heat Recovery Systems and CHP* 13.2 (1993), pp. 147–159. DOI: https://doi.org/10.1016/0890-4332(93)90034-S. URL: https://www.sciencedirect.com/science/article/pii/089043329390034S.

[14] Marcel Ahrens, A. Hafner, and Trygve Eikevik. “Development of Ammonia-Water Hybrid Absorption-Compression Heat Pumps”. In: Aug. 2019. DOI: 10.18462/iir.icr.2019.1869.

[15] O Brunin, M Feidt, and B Hivet. “Comparison of the working domains of some compression heat pumps and a compression-absorption heat pump”. In: *International Journal of Refrigeration* 20.5 (1997), pp. 308–318. DOI: https://doi.org/10.1016/S0140-7007(97)00025-X. URL: https://www.sciencedirect.com/science/article/pii/S014070079700025X.

[16] Jonas K. Jensen, Lars Reinholdt, Wiebke B Markussen, and Brian Elmegaard. “Investigation of ammonia/water hybrid absorption/compression heat pumps for heat supply temperatures above 100 °C”. In: *Proceedings of the International Sorption Heat Pump Conference* 1 (2014), pp. 311–320.

[17] D.M. van de Bor, C.A. Infante Ferreira, and Anton A. Kiss. “Low grade waste heat recovery using heat pumps and power cycles”. In: *Energy* 89 (2015), pp. 864–873. DOI: https://doi.org/10.1016/j.energy.2015.06.030. URL: https://www.sciencedirect.com/science/article/pii/S0360544215007860.

[18] Chun Qing, Peng Gao, and Chun-Lu Zhang. “Thermodynamic analysis on feasible operating region of two-stage hybrid absorption-compression heat pump cycles”. In: *International Journal of Refrigeration* 121 (2021), pp. 43–50. DOI: https://doi.org/10.1016/j.ijrefrig.2020.09.017. URL: https://www.sciencedirect.com/science/article/pii/S0140700720303893.

[19] AA Kiss and Carlos Infante Ferreira. *Heat Pumps in Chemical Process Industry*. English. CRC Press / Balkema - Taylor & Francis Group, 2016.

[20] Gy. Bergmann and G. Hivessy. “Experimental Hybrid Heat Pump of 1000kW heating capacity”. In: *Applications and Efficiency of Heat Pump Systems*. Ed. by I. E. Smith. Berlin, Heidelberg: Springer Berlin Heidelberg, 1991, pp. 27–40.

[21] L.C.M. Itard. “Wet compression-resorption heat pump cycles: Thermodynamic analysis and design”. PhD thesis. Delft University of Technology, 1998.

[22] D.V. Zaytsev. “Development of wet compressor for application in compression-resorption heat pumps”. PhD thesis. Delft University of Technology, 2003.

[23] C.A. Infante Ferreira, C. Zamfirescu, and D. Zaytsev. “Twin screw oil-free wet compressor for compression–absorption cycle”. In: *International Journal of Refrigeration* 29.4 (2006), pp. 556–565. DOI: https://doi.org/10.1016/j.ijrefrig.2005.10.006. URL: https://www.sciencedirect.com/science/article/pii/S0140700705002008.

[24] V. Guðjónsdóttir. “Upgrading waste heat streams with wet compression”. PhD thesis. Delft University of Technology, 2020.

[25] V.V. Kothari. “Experimental Validation of Wet Compression with a Twin Screw Compressor Prototype”. Master Thesis. Delft University of Technology, 2020.

[26] K. Guðmundsdóttir. “Wet compression with a twin screw compressor prototype”. Master Thesis. Delft University of Technology, 2018.

[27] Yan Tang. “Computer aided design of twin screw compressors”. Thesis. 1995. DOI: http://localhost/files/td96k256m.

[28] L.L. van Bommel. “Thermodynamic Model of a Screw Compressor”. Master Thesis. Delft University of Technology, 2016.

[29] M. Brancaccio. “Modelling of wet compression in compression-resorption heat pumps”. Master Thesis. Delft University of Technology, 2023.

[30] V. Gudjonsdottir, C.A. Infante Ferreira, V. Kothari, and A. Goethals. “Experimental performance of a wet compressor operating with ammonia-water under high temperature compression-resorption heat pump conditions”.

[31] Fourth Utility Consulting Brian Parks. *Isentropic Efficiency of rotary Screw Air Compressors*. URL: https://www.airbestpractices.com/standards/iso-and-cagi/isentropic-efficiency-rotary-screw-air-compressors#:~:text=Air%20Compressor%20Isentropic%20Efficiency&text=The%20calculation%20is%20(total%20package,same%20full%20load%20pressure%20rating.. (accessed: 27.10.2023.

[32] V. Gudjonsdottir, C.A. Infante Ferreira, and A. Goethals. “Wet compression model for entropy production minimization”. In: *Applied Thermal Engineering* 149 (2019), pp. 439–447. DOI: https://doi.org/10.1016/j.applthermaleng.2018.12.065. URL: https://www.sciencedirect.com/science/article/pii/S1359431118336743.

[33] Marcel Ulrich Ahrens, Ignat Tolstorebrov, Even Kristian Tønsberg, Armin Hafner, R.Z. Wang, and Trygve Magne Eikevik. “Numerical investigation of an oil-free liquid-injected screw compressor with ammonia-water as refrigerant for high temperature heat pump applications”. In: *Applied Thermal Engineering* 219 (2023), p. 119425. DOI: https://doi.org/10.1016/j.applthermaleng.2022.119425. URL: https://www.sciencedirect.com/science/article/pii/S1359431122013552.

[34] Yafen Tian, Hao Yuan, Chuang Wang, Huagen Wu, and Ziwen Xing. “Numerical investigation on mass and heat transfer in an ammonia oil-free twin-screw compressor with liquid injection”. In: *International Journal of Thermal Sciences* 120 (2017), pp. 175–184. DOI: https://doi.org/10.1016/j.ijthermalsci.2017.06.007. URL: https://www.sciencedirect.com/science/article/pii/S1290072917302570.

[35] Sylvain Quoilin. “Sustainable energy conversion through the use of Organic Rankine Cycles for waste heat recovery and solar applications”. English. PhD thesis. ULiège - Université de Liège, 4October 2011.

[36] Sebastian Araya, Aaron P. Wemhoff, Gerard F. Jones, and Amy S. Fleischer. “An experimental study of an Organic Rankine Cycle utilizing HCFO-1233zd(E) as a drop-in replacement for HFC-245fa for ultra-low-grade waste heat recovery”. In: *Applied Thermal Engineering* 180 (2020), p. 115757. DOI: https://doi.org/10.1016/j.applthermaleng.2020.115757. URL: https://www.sciencedirect.com/science/article/pii/S1359431120332397.

[37] F García, R García, J.C Padrino, C Mata, J.L Trallero, and D.D Joseph. “Power law and composite power law friction factor correlations for laminar and turbulent gas–liquid flow in horizontal pipelines”. In: *International Journal of Multiphase Flow* 29.10 (2003), pp. 1605–1624. DOI: https://doi.org/10.1016/S0301-9322(03)00139-3. URL: https://www.sciencedirect.com/science/article/pii/S0301932203001393.

[38] D. Chisholm. “Two-phase flow in bends”. In: *International Journal of Multiphase Flow* 6.4 (1980), pp. 363–367. DOI: https://doi.org/10.1016/0301-9322(80)90028-2. URL: https://www.sciencedirect.com/science/article/pii/0301932280900282.

[39] VDI Gesellschaft. *VDI Heat Atlas*. VDI-Buch. Springer Berlin Heidelberg, 2010, p. 1067. URL: https://books.google.nl/books?id=0t-HrUf1aHEC.

[40] G.B. Wallis, J.G. Collier, Stanford University, Stanford University. Department of Mechanical Engineering, and Dartmouth College. *Two-phase Flow and Heat Transfer: Notes for a Summer Course July 24-August 4, 1967, Department of Mechanical Engineering, Stanford University, Stanford, California*. Two Phase Flow and Heat Transfer v. 3. Stanford University, 1967. URL: https://books.google.nl/books?id=tykkAQAAIAAJ.

[41] W.H. McAdams and National Research Council (U.S.). Committee on Heat Transmission. *Heat Transmission*. Chemical engineering series. McGraw-Hill, 1942. URL: https://books.google.nl/books?id=tMogAAAAMAAJ.

[42] The Engineering ToolBox. *Dynamic Viscosity of Motor Oils*. https://www.engineeringtoolbox.com/dynamic-viscosity-motor-oils-d_1759.html. Accessed: 2024-07-03.

[43] The Engineering ToolBox. *Specific Heat of Liquids and Fluids*. https://www.engineeringtoolbox.com/specific-heat-fluids-d_151.html. Accessed: 2024-07-03.

[44] The Engineering ToolBox. *Thermal Conductivity*. https://www.engineeringtoolbox.com/thermal-conductivity-d_429.html. Accessed: 2024-07-03.

[45] The Engineering ToolBox. *Densities of Common Liquids*. https://www.engineeringtoolbox.com/liquids-densities-d_743.html. Accessed: 2024-07-03.

[46] Michel D. Obrist, Ramachandran Kannan, Thomas J. Schmidt, and Tom Kober. "Long-term energy efficiency and decarbonization trajectories for the Swiss pulp and paper industry". In: *Sustainable Energy Technologies and Assessments* 52 (2022), p. 101937. DOI: https://doi.org/10.1016/j.seta.2021.101937. URL: https://www.sciencedirect.com/science/article/pii/S2213138821009516.

[47] United States Environmental Protection Agency. *Environmental Factoids*. https://archive.epa.gov/epawaste/conserve/smm/wastewise/web/html/factoid.html. Accessed: 2024-06-22. June 2024.

[48] Luis Miguel Calvo and Rosario Domingo. "CO2 Emissions Reduction and Energy Efficiency Improvements in Paper Making Drying Process Control by Sensors". In: *Sustainability* 9.4 (2017). DOI: 10.3390/su9040514. URL: https://www.mdpi.com/2071-1050/9/4/514.

[49] Statistics Netherlands (CBS). *Energy Balance Sheet; Supply, Transformation and Consumption*. Accessed: 2024-08-11. 2024. URL: https://www.cbs.nl/en-gb/figures/detail/85666ENG.

[50] Trading Economics. *Carbon permits EU*. https://tradingeconomics.com/commodity/carbon. Accessed: 2024-08-11.

[51] AA Kiss and Carlos Infante Ferreira. *Heat Pumps in Chemical Process Industry*. English. CRC Press / Balkema - Taylor Francis Group, 2016.

[52] U.S. Bureau of Labor Statistics. *Producer Price Index by Industry: Total Manufacturing Industries (PCUOMFGOMFG)*. Retrieved July 12, 2024. Index Dec 1984=100, Not Seasonally Adjusted, Monthly. 2024. URL: https://fred.stlouisfed.org/series/PCUOMFGOMFG.

[53] Jibran Zuberi, Ali Hasanbeigi, and William Morrow. "Electrification of industrial boilers in the USA: potentials, challenges, and policy implications". In: *Energy Efficiency* 15 (Dec. 2022). DOI: 10.1007/s12053-022-10079-0.

[54] E. W. Lemmon, I. H. Bell, M. L. Huber, and M. O. McLinden. *NIST Standard Reference Database 23: Reference Fluid Thermodynamic and Transport Properties-REFPROP, Version 10.0, National Institute of Standards and Technology*. 2024. DOI: https://doi.org/10.18434/T4/1502528. URL: https://www.nist.gov/srd/refprop.

[55] Engineering ToolBox. *Refrigerants - Environmental Properties*. Accessed: 2024-07-18. 2024. URL: https://www.engineeringtoolbox.com/Refrigerants-Environment-Properties-d_1220.html.

[56] Øivind Hodnebrog, Stig B. Dalsøren, and Gunnar Myhre. "Lifetimes, direct and indirect radiative forcing, and global warming potentials of ethane (C2H6), propane (C3H8), and butane (C4H10)". In: *Atmospheric Science Letters* 19.2 (2018), e804. DOI: https://doi.org/10.1002/asl.804. URL: https://rmets.onlinelibrary.wiley.com/doi/abs/10.1002/asl.804.

[57] Cooling Post. *New HCFO Refrigerant ASHRAE Listed*. Accessed: 2024-07-18. 2024. URL: https://www.coolingpost.com/world-news/new-hcfo-refrigerant-ashrae-listed/.

[58] Honeywell International Inc. *HFC-245fa Product Stewardship Summary*. Accessed: 2024-07-18. Dec. 2007.

[59] United Nations Environment Programme. *Montreal Protocol on Substances that Deplete the Ozone Layer: 2006 Report of the Rigid and Flexible Foams Technical Options Committee*. Nairobi, Kenya: United Nations Environment Programme, 2006.

A

Work on experimental setup

A.1. Preparation of setup

Since the setup was last used there has been maintenance in the Process and Energy Lab. To facilitate this the setup had to be disassembled and stored outside. In order to perform experiments again the setup first has to be commissioned. First the setup needed to be assembled. The correct assembly had to be verified by leak testing the setup. Once the setup was leak free it was insulated. Lastly the computer had to be upgraded and the compressor needed to be revised.

A.1.1. Assembly of the setup

Before the start of this thesis a lot of effort went in to the correct assembly of the setup. A few modifications needed to be made to get everything aligned and connected correctly. The floor of the lab was altered which resulted in a misalignment. The setup also has some modifications including a valve and a pressure gauge at the gap seal of the compressor and the addition of a temperature sensor at the separator.

A.1.2. Leak testing of the setup

The setup has been pressurized to 8.5 bar to see if there are any significant leaks. First the entire system was pressurized using nitrogen. In order to determine the location of possible leaks three valves were closed which sub-divided the system as shown in figure A.1. After tightening of some of the connections part A and C of the setup were able to hold the pressure for over two months without losing a significant amount of pressure and were considered leak free. Part B of the setup, the compressor, was leaking at a large rate. This meant that the system would be near atmospheric pressure within 24 hours.

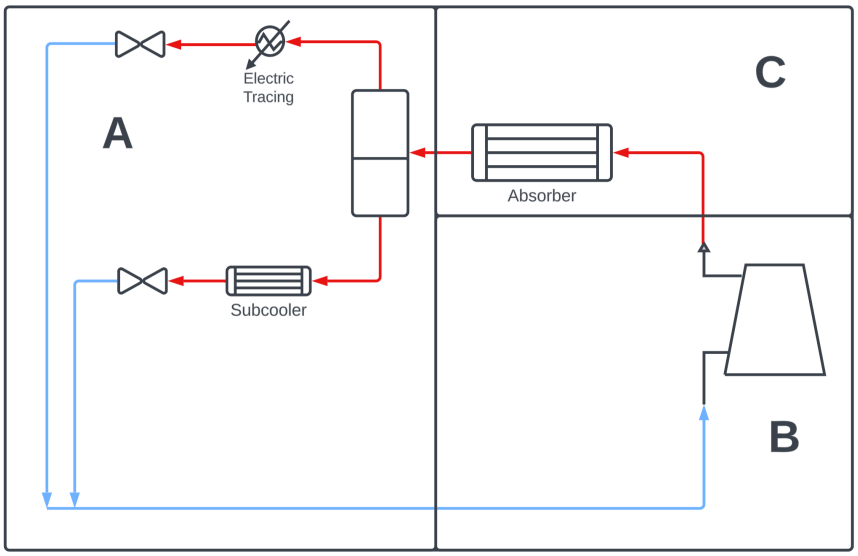

Figure A.1: The three segments that were leak tested

A.1.3. Insulating of the setup

Due to the high temperatures of the setup it has to be insulated to reduce heat loss to the environment affecting measurements. This was done by the use of ROCKWOOL with 50 mm thickness for the piping. The compressor side still remains to be insulated in order to operate. This will be done after part B of the setup has been leak tested and is functional.

A.1.4. The computer has been upgraded

In order to operate the setup as well as to measure and log the results a computer is attached to a CompactRio 9066 which is connected to the sensors and valves of the setup. After the rebuild of the setup the software on the old computer was not compatible with the current licensed software versions. In order to resolve this the computer was replaced and reconfigured. The password that was used to access the software from the CompactRio was lost. In order to install the correct software the controller was put back to factory defaults and the correct software was installed.

A.1.5. Compressor revision

The disassembly and storage of the compressor resulted in leaks at the compressor side of the setup. Additionally the window is in the compressor gearbox that allows to see the oil level broke in September. This resulted in a large oil spill. Atlas Copco decided that it was best to remove the compressor and inspect it. During inspection it became clear that the compressor core had corroded which resulted in difficulties to get the compressor leak tight.

B

Case study

B.1. Working fluid VCHP

The selection of a working fluid is based on the following criteria:

- Low GWP
- Zero ODP
- Acceptable pressure on high pressure side
- Above atmospheric pressure on low pressure side
- Enable small equipment size

A low equipment size will be achieved when the vapor density times the heat of vaporization is higher. The working fluids were selected by reviewing selecting refrigerants which have a boiling point below the low temperature of the heat pump and a critical temperature higher than the hot temperature of the heat pump. Water and ammonia are also included since these are are used in the HACHP and CRHP.

Working fluid comparison

In table B.1 the important properties and relevant pressures at the low and high temperatures as described in section 6.2.1 are defined. Here boiling point is considered at 1 bar and heat of evaporation and vapor density at 1 bar and $20\,^{\circ}$C. Where not mentioned thermodynamic properties were obtained from Refprop [54].

Table B.1: Properties of potential working fluids

Working fluid	GWP	ODP	Boiling point	Critical temperature	$h_{evap} \cdot \rho_V$	Pressure at $15\,^{\circ}$C	Pressure at $140\,^{\circ}$C
Ammonia	0 [55]	0 [55]	239.6 K	405.6 K	1.04 MJ/m^3	7.3 bar	-
Water	0 [55]	0 [55]	372.8 K	647.1 K	1.4 MJ/m^3	0.017 bar	3.6 bar
Butane	6.5 [56]	0 [56]	272.3 K	425.1 K	0.98 MJ/m^3	1.8 bar	31 bar
R-1224yd(Z)	0.00012 [57]	<1 [57]	287.4 K	428.7 K	1.1 MJ/m^3	1.0 bar	25 bar
R-245fa	950 [58]	0 [59]	287.9 K	427.0 K	1.1 MJ/m^3	1.0 bar	28 bar

Here it can be seen that is not possible to have a sub-critical VCHP with ammonia at these temperatures. Butane, R-1224yd(Z) and R-245fa are all suitable for a VCHP operating at the described temperatures. Butane is selected because it has an acceptable GWP while also having the lowest pressure ratio which will reduce the equipment cost.

B.2. Governing equations VCHP

In order to calculate the state temperatures a hot and cold temperature T_{hot} and T_{cold} will be chosen. These temperatures are the design temperatures for the waste heat streams at the condenser and absorber outlets respectively. The other input parameters are T_{wh}, the waste heat temperature and T_{dr} the minimum driving force in the heat exchangers. In order to design the cycle, the temperatures and pressures at the absorber outlet are calculated as follows:

$$T_1 = T_{cold} - T_{dr} \tag{B.1}$$

$$p_1 = f(T_1, q = 1) \tag{B.2}$$

$$s_1 = f(T_1, p_1) \tag{B.3}$$

The pressure of the hot side follows from the condenser outlet properties as described in equation B.4.

$$p_3 = f(T_3, q = 0) \tag{B.4}$$

Where T_3 is calculated using equation B.5.

$$T_3 = T_{hot} + T_{dr} \tag{B.5}$$

Since the condensing and evaporating happens at constant temperature and pressure:

$$p_2 = p_3 \tag{B.6}$$

$$T_4 = T_1, p_4 = p_1 \tag{B.7}$$

For $i = 1, 3, 4$ the state enthalpies can calculated by the use of Refprop [54] using equation B.8.

$$h_i = f(T_i, p_i) \tag{B.8}$$

In order to calculate the temperature at point 2 first the isentropic enthalpy is calculated using equation B.9. Using this enthalpy the enthalpy at point 2 is calculated using equation B.10 and finally the temperature using equation B.11

$$h_{2,is} = f(s_1, p_2) \tag{B.9}$$

$$h_2 = h_1 + \frac{h_{2,is} - h_1}{\eta_{is}} \tag{B.10}$$

$$T_2 = f(h_2, p_2) \tag{B.11}$$

The heat taken in by the evaporator is calculated using equation B.12 and the heat released by the condenser is calculated using B.13.

$$\dot{Q}_{source} = \dot{m} \cdot (h_1 - h_4) \tag{B.12}$$

$$\dot{Q}_{sink} = \dot{m} \cdot (h_3 - h_2) \tag{B.13}$$

B.3. Governing equation CRHP

The CRHP is used to upgrade the waste heat. The input parameters chosen are:

- Thermal driving force
- Waste heat temperature
- Total ammonia concentration
- Compressor inlet vapor quality
- Absorber outlet quality

The thermal driving force impacts both the energetic and the economic performance of the heat pump. The cycle will be evaluated for different values of T_{dr}. The waste heat temperature is fixed at 60 K. The adjusting of the total ammonia concentrations effects the operating window of the heat pump and is the parameter that is varied in order to evaluate the heat pump performance at different upgraded waste heat temperatures. The cycle performance will be evaluated for total ammonia concentrations from 0.15 to 0.85 wt%. The compressor inlet vapor quality is fixed at 80 %. This value was chosen to ensure that enough

liquid was present throughout the compressor for the sealing and cooling of the compressor. It is assumed that the mixture is completely condensed at the absorber outlet, this leaves the most opportunity for heat transfer to and from the working fluid.

The states considered are as displayed in figure 6.5. Since the waste heat streams are in a counter-current configuration the temperatures at point 1 and point 3 can be calculated using equation B.14 and B.15.

$$T_1 = T_{wh} - T_{dr} \tag{B.14}$$

$$T_3 = T_{wh} + T_{dr} \tag{B.15}$$

Using these temperatures the low and high pressures from the cycle can be calculated using equation B.16 and equation B.17.

$$p_1 = f(T_1, q = 0.8, X_T) \tag{B.16}$$

$$p_3 = f(T_3, q = 0, X_T) \tag{B.17}$$

The pressure drop over the heat exchangers is considered to be negligible. This gives $p_2 = p_3$ and $p_4 = p_1$. The expansion is assumed isenthalpic resulting in $h_4 = h_3$. Using this the temperature at point 4 can be calculated using equation B.18.

$$T_4 = f(p_4, h_4, X_T) \tag{B.18}$$

In order to determine the properties at point 2 first the enthalpy and entropy at point 1 are calculated using equation B.19.

$$s_1, h_1 = f(T_1, q = 0.8, X_T) \tag{B.19}$$

This enables the calculation of the isentropic enthalpy at point 2 as calculated in equation B.20.

$$h_{2,is} = f(p_2, s_1, X_T) \tag{B.20}$$

Finally the enthalpy at point 2 can be calculated using equation B.21 and with that the temperature at point 2 is calculated using equation B.22.

$$h_2 = h_1 + \frac{h_{2,is} - h_1}{\eta_{is}} \tag{B.21}$$

$$T_2 = f(p_2, h_2, X_T) \tag{B.22}$$

To evaluate the energetic performance of the cycle the COP is of interest. This is calculated using equation B.23. The heat transferred to the working fluid at the source is calculated using equation B.24 and the heat rejected by the working fluid at the heat sink is calculated using equation B.25.

$$COP = \frac{h_2 - h_3}{h_2 - h_1} \tag{B.23}$$

$$Q_{source} = \dot{m} \cdot (h_1 - h_4) \tag{B.24}$$

$$Q_{sink} = \dot{m} \cdot (h_2 - h_3) \tag{B.25}$$

B.4. Economic calculation VCHP

Table B.2: Economic performance of VCHP

T_{dr}	5 K	10 K
COP	2.01	1.72
$\dot{Q}_{source}$	0.50 MW	0.42 MW
$T_{ln,source}$	5 K	10 K
U-value source	1200 W/(m^{2}K)	1200 W/(m^{2}K)
Area source	84 m^2	35 m^2
Cost heat exchanger source	77 k€	35 k€
$\dot{Q}_{sink}$	1.0 MW	1.0 MW
$T_{ln,sink}$	5 K	10 K
U-value sink	1500 W/(m^{2}K)	1500 W/(m^{2}K)
Area sink	133 m^2	67 m^2
Cost heat exchanger sink	120 k€	63 k€
Cost compressor	1343 k€	1518 k€
Investment cost	1540 k€	1616 k€
Yearly savings	256 k€	44 k€
Payback time	6.0 years	36.7 years

B.5. Economic calculation CRHP

In this section the economic performance of the CRHP will be analysed for this analysis the method proposed by Kiss and Infante Ferreira is used [51]. The results and assumptions are shown in table B.3

Table B.3: Economic performance of CRHP

T_{dr}	5 K	5 K	10 K	10 K
COP	3.36-3.96	3.31-3.56	3.05-3.46	2.75-3.09
X_T	0.37-0.41	0.82-0.80	0.30-0.40	0.83-0.80
$\dot{Q}_{source}$	0.70−0.75 MW	0.67−0.71 MW	0.70−0.72 MW	0.64−0.68 MW
$\Delta T_{ln,source}$	5 K	5 K	10 K	10 K
U-value source	1000 W/(m^{2}K)	1000 W/(m^{2}K)	1000 W/(m^{2}K)	1000 W/(m^{2}K)
Area source	141−149 m^2	134−142 m^2	70−72 m^2	64−68 m^2
Cost heat exchanger source	126 − 133 k€	120 − 127 k€	65 − 67 k€	60 − 63 k€
$\dot{Q}_{sink}$	1.0 MW	1.0 MW	1.0 MW	1.0 MW
$\Delta T_{ln,source}$	5 K	5 K	10 K	10 K
U-value sink	1000 W/(m^{2}K)	1000 W/(m^{2}K)	1000 W/(m^{2}K)	1000 W/(m^{2}K)
Area sink	200 m^2	200 m^2	100 m^2	100 m^2
Cost heat exchanger sink	175 k€	175 k€	91 k€	91 k€
Cost compressor	2080 − 1830 k€	1934 − 1750 k€	2106 − 1990 k€	2098 − 1934 k€
Investment cost	2378 − 2138 k€	2229 − 2052 k€	2262 − 2148 k€	2249 − 2088 k€
Yearly savings	762 − 876 k€	751 − 805 k€	686 − 784 k€	595 − 696 k€
Payback time	3.1-2.4 years	3.0-2.6 years	3.2-2.7 years	3.8-3.0 years

As concluded in section 6.2.1 the ammonia rich CRHP solutions have a significant lower pressure drop. To account for this the ammonia lean CRHP solutions were assumed to require two stage compression

resulting in two compressors rated for half the power.